Available online at www.sciencedirect.com
SCIENCE DIRECT®
Journal of Computational Physics 202 (2005) 94–133
JOURNAL OF COMPUTATIONAL PHYSICS
www.elsevier.com/locate/jcp

Variational multiscale stabilized FEM formulations for transport equations: stochastic advection–diffusion and incompressible stochastic Navier–Stokes equations

Velamur Asokan Badri Narayanan, Nicholas Zabaras *

Materials Process Design and Control Laboratory, Sibley School of Mechanical and Aerospace Engineering, Cornell University, Ithaca, NY 14853-3801, USA

Received 8 January 2004; received in revised form 28 May 2004; accepted 23 June 2004
Available online 26 August 2004

Abstract

An extension of the deterministic variational multiscale (VMS) approach with algebraic subgrid scale (SGS) modeling is considered for developing stabilized finite element formulations for the stochastic advection and the incompressible stochastic Navier–Stokes equations. The stabilized formulations are numerically implemented using the spectral stochastic formulation of the finite element method (SSFEM). Generalized polynomial chaos and Karhunen–Loève expansion techniques are used for representation of uncertain quantities. The proposed stabilized method is then applied to various standard advection–diffusion and fluid-flow examples with uncertainty in essential boundary conditions. Comparisons are drawn between the numerical solutions and Monte-Carlo/analytical solutions wherever possible.
© 2004 Elsevier Inc. All rights reserved.

Keywords: Variational multiscale; Spectral stochastic FEM; Polynomial chaos; Stochastic advection; Stochastic fluid-flow; Subgrid scale models; Karhunen–Loève expansion; Monte-Carlo

1. Introduction

In the past decade, there has been a considerable interest in solving realistic problems of transport and fluid flow. A majority of these problems can be modeled with the advection–diffusion and the incompressible Navier–Stokes equations. Numerical solution of these equations presents difficulties in the presence of boundary

* Corresponding author. Tel.: +1 607 255 9104; fax: +1 607 255 1222.
E-mail address: zabaras@cornell.edu (N. Zabaras).

0021-9991/$ - see front matter © 2004 Elsevier Inc. All rights reserved.
doi:10.1016/j.jcp.2004.06.019

or internal layers where sharp gradients can occur in the solution due to high Péclet numbers and/or Reynolds numbers. Further errors are introduced due to phase, amplitude errors and pollution of the solution due to excess diffusion. A majority of the devoted research effort in this area has been directed towards solution of these problems under the assumption of ideal input (precise inlet boundary conditions, initial conditions, material properties and computational domain). In practice, this is hardly the case and the input is always polluted with uncertainties. This necessitates stochastic approaches for modeling fluid flow and transport.

In this context, the perturbation method and the method of moments have been successfully applied to analyze flow in porous media, contaminant transport and problems related to groundwater transport [1–3]. Sensitivity derivatives have also been used for investigating free-convection [4], the k-ε turbulence model and supersonic flow [5–7]. However, these methods are limited to small fluctuations and do not provide detailed information about higher order statistics of the solution. Further, the perturbation method can become intractable for moments of order greater than two. The Monte-Carlo method can be applied but is computationally expensive and can become unrealistic even for simple flow problems. A more effective approach based on the spectral representation of uncertainty was introduced by Ghanem and Spanos [8] wherein the stochastic solution is represented as a sum of projections on an appropriate Hilbert space of random variables. Such a representation was shown to converge to the exact stochastic solution in the L_2 sense [9] and hence, in probability distribution. This approach known popularly as the spectral stochastic approach has been successfully used to investigate stochastic transport and fluid-flow problems using finite-differences [10–12] and flow in random media [13]. The spectral stochastic approach in conjunction with the spectral FEM has been applied to flow-structure interactions and stochastic advection [14–16]. However, all these techniques do not fall under the category of Galerkin finite elements that require stabilization.

Stabilized finite elements for fluid-flow and transport have grown in popularity over the last two decades starting from the initial techniques like SUPG, Galerkin least squares (GLS), the SUPG-PSPG method [17–20] up to the more recent residual free bubbles, subgrid scale models and the variational multiscale framework [21–25]. In this context, it is also worth mentioning the multiscale finite element method developed in [26–28]. The variational multiscale method has been used for large eddy simulation of turbulent flows [29–31]. It provides a mathematically rigorous framework for stabilization of convection dominant flows. It unifies the concepts of residual free bubbles, subgrid scale models and Green's functions and encompasses other stabilization techniques like SUPG, SUPG-PSPG and GLS. The purpose of this paper is to integrate the variational multiscale method in a spectral stochastic approach to derive stabilized FEM formulations for the stochastic advection–diffusion and incompressible stochastic Navier–Stokes equations.

The paper is organized as follows. We begin in Section 2 with a brief introduction to the spectral stochastic framework. In Sections 3 and 4, the definitions of scalar stochastic advection–diffusion and incompressible stochastic Navier–Stokes equations are considered, respectively. The variational multiscale framework for deriving a stabilized framework for the solution of the above equations is also presented. Following this, Section 5 presents some details of the finite element implementation of the spectral stochastic framework. Several numerical examples are considered in Section 6 to validate the accuracy, convergence and efficiency of the proposed scheme in the context of steady and transient advection–diffusion problems and standard benchmark fluid-flow examples. Finally, in Section 7, the paper concludes with a brief summary of inferences and suggestions for future investigation.

2. Stochastic framework and spectral approach

2.1. Probability space and spectral representations

Let $(\Omega, \mathscr{F}, \mathscr{P})$ be a probability space, where Ω is the space of basic outcomes, $\mathscr{F}$ is the minimal σ-algebra of the subsets of Ω and $\mathscr{P}$ is the probability measure on $\mathscr{F}$. The σ-algebra $\mathscr{F}$ can be viewed as a collection

of all possible events that can be derived from the basic outcomes in Ω and have a well defined probability with respect to $\mathscr{P}$. The notation ω will be used to refer to the basic outcomes in the sample space, i.e., $\omega \in \Omega$ [32].

In this framework, a real-valued random variable X is defined as a function that maps the probability space to the real line or a subset of the real line. In short $\quad : (\Omega, \mathscr{F}, \mathscr{P}) \mapsto \mathbb{R}$. The expected value of X, when it exists, is denoted as

$$E \quad = \int_{\Omega} \quad (\omega) \mathrm{d}\mathscr{P}(\omega) = \int_{\mathbb{R}} \quad \mathrm{d}F(\quad), \tag{1}$$

where $F(x)$ is the probability distribution measure for X defined on the real line $\mathbb{R}$ or a part of it [33]. Further, a part of the real line denoted as $\mathbb{B}$ can be mapped back to the sample space via $\quad^{-1}(\mathbb{B})$ and the following probability relation holds:

$$F(\mathbb{B}) = \mathscr{P}(\quad^{-1}(\mathbb{B})). \tag{2}$$

We will assume in all of our work that $F(x)$ is continuous (or with finite discontinuities) with respect to the Lebesgue measure. This justifies the usage of probability density/mass functions for stochastic quantities and it is a reasonable assumption for most continuum quantities of interest (such as velocity, temperature, pressure and other).

The space of all second-order random variables is denoted by $L_2(\Omega, \mathscr{F}, \mathscr{P})$ and is defined as the Hilbert space formed by random variables $X(\omega)$ equipped with the mean-square norm

$$\| \quad (\omega)\|_{L_2(\Omega)} = (E \mid \quad (\omega)|^2)^{1/2} < \infty. \tag{3}$$

For notational convenience, we shall refer to $L_2(\Omega, \mathscr{F}, \mathscr{P})$ as $L_2(\Omega)$ with the understanding that $L_2(\Omega) = \{X(\omega) : E|X(\omega)|^2 < \infty\}$. It can also be shown that $L_2(\Omega)$ is complete [33]. Thus, any random variable $X(\omega) \in L_2(\Omega)$ can be expressed as a summation

$$(\omega) = \sum_{=0}^{\infty} \quad \zeta\,(\omega), \tag{4}$$

where $\boldsymbol{\zeta} = \{\zeta\,(\omega)\}_0^{\infty}$ form a basis of $L_2(\Omega)$ and $\{\quad\}_0^{\infty}$ denote the projections of $X(\omega)$ onto the basis $\boldsymbol{\zeta}$. We can also extend Eq. (4) to include space-time stochastic processes with finite second moment at each point in space and time

$$(\mathbf{x}, \ , \omega) = \sum_{=0}^{\infty} \quad (\mathbf{x}, \ )\zeta\,(\omega). \tag{5}$$

2.2. Finite dimensional subspaces of $L_2(\Omega)$ and spectral approximation of stochastic quantities

Eq. (4) involves an infinite summation and hence is computationally intractable. Therefore, we consider finite-dimensional subspaces of $L_2(\Omega)$ that best represent the uncertainty in $X(\omega)$. Such subspaces can be defined by an appropriate choice of basis. The most popular methods for choosing the basis are as follows:

Karhunen–Loève expansion (*KLE*): The KLE for a stochastic process $W(\mathbf{x},t,\omega)$ is based on the spectral decomposition of its covariance function $R_{\mathrm{hh}}(\mathbf{y}_1,\mathbf{y}_2)$. Here, $\mathbf{y}_1$ and $\mathbf{y}_2$ denote the spatio-temporal coordinates (x_1,t_1) and (x_2,t_2), respectively. By definition, the covariance function is symmetric and positive definite and has real positive eigenvalues. Further, all its eigenfunctions are orthogonal and span the space to which $W(\mathbf{x},t,\omega)$ belongs. The expansion can be written as

$$(\mathbf{x}, \ , \omega) = E \quad (\mathbf{x}, \ ) + \sum_{=0}^{\infty} \sqrt{\lambda}\,\phi\,(\mathbf{x}, \ )\xi\,(\omega), \tag{6}$$

where $EW(\mathbf{x},t)$ denotes the mean of the process and $\{\xi(\omega)\}_0^\infty$ forms a set of uncorrelated random variables whose distribution has to be determined [32]. Also $\{\xi(\omega)\}_0^\infty$ span $L_2(\Omega)$. $\{\phi(\mathbf{x},\ )\}_0^\infty$ and $\{\lambda\}_0^\infty$ form the eigenpairs of the covariance function, i.e.

$$\int_{(\mathscr{D}\times\mathscr{T})} \text{hh}(\mathbf{y}_1,\mathbf{y}_2)\phi(\mathbf{y}_2)\mathrm{d}\mathbf{y}_2 = \lambda\,\phi(\mathbf{y}_1), \tag{7}$$

where $\mathscr{D}$ and $\mathscr{T}$ denote the spatial and temporal domains, respectively. The chief characteristic of the KLE is that the spatio-temporal randomness has been decomposed into a set of deterministic functions multiplying random variables. These deterministic functions can also be thought of as representing the scales of fluctuations of the process. The KLE is mean-square convergent to the original process $W(\mathbf{x},t,\omega)$ provided the process has finite variance. The expansion in Eq. (6) is typically truncated to a finite number of summation terms. The closer a process is to white noise, the more the number of terms needed for approximation, on the other hand a random variable requires just one term in the KLE. The main disadvantage of this technique is that it requires knowledge of the covariance function. This is typically not available especially for the solution of a coupled system of stochastic partial differential equations. Thus, we consider the generalized polynomial chaos expansion approach that is discussed next.

Generalized polynomial chaos expansion (*GPCE*): The original Wiener polynomial chaos employs Hermite polynomials in multi-dimensional Gaussian random variables as the trial basis for $L_2(\Omega)$ [34]. Cameron and Martin [9] proved that such a choice of basis leads to an expansion that is convergent in mean-square sense to the original process. The Wiener-polynomial chaos expansion for a second-order random variable can be written as follows:

$$(\omega) = \ _0\ \ _0 + \sum_{_1=1}^{\eta} \ _1H_1(\xi_{_1}(\omega)) + \cdots + \sum_{_1=1}^{\eta}\cdots\sum_{_\eta=1}^{\eta-1} \ _{1\,2,\ldots,\eta}H_{\eta}(\xi_{_1}(\omega),\ldots,\xi_{_\eta}(\omega)) + \cdots \tag{8}$$

where $H_n(\xi_{i_1}(\omega),\ldots,\xi_{i_n}(\omega))$ denote Hermite polynomials of order (n) in independent identically distributed Gaussian random variables $\boldsymbol{\xi} = (\xi_1,\ldots,\xi_n)$ [8,34]. The general expression for the Hermite polynomials is given as

$$H_{\eta}(\xi_{_1}(\omega),\ldots,\xi_{_\eta}(\omega)) = \exp\left(\frac{1}{2}\boldsymbol{\xi}^{\mathrm{T}}\boldsymbol{\xi}\right)(-1)^{\eta}\frac{\partial^{\eta}}{\partial\xi_{_1}\ldots\partial\xi_{_\eta}}\exp\left(-\frac{1}{2}\boldsymbol{\xi}^{\mathrm{T}}\boldsymbol{\xi}\right), \tag{9}$$

where $i_1 + i_2 + \cdots + i_n = n$.

For notational convenience, we rewrite Eq. (8) as

$$(\omega) = \sum_{_\iota=0}^{\infty} \hat{}_{\iota}\,\psi_{\iota}(\boldsymbol{\xi}). \tag{10}$$

There is a one-to-one correspondence between $H_n(\boldsymbol{\xi})$ and $\psi_j(\boldsymbol{\xi})$. The set of polynomials $\{\psi_{\iota}(\boldsymbol{\xi})\}_0^\infty$ form a complete orthogonal basis spanning $L_2(\Omega)$. The orthogonality relation can be expressed as

$$E[\psi(\boldsymbol{\xi})\psi_{\iota}(\boldsymbol{\xi})] = E[\psi(\boldsymbol{\xi})^2]\delta_{\iota}, \tag{11}$$

where δ_{ij} is the Kronecker delta operator, and the expectation operator is defined along the same lines as in Eq. (1). It should be noted here that since $\boldsymbol{\xi}$ is a vector of n-uncorrelated Gaussian random variables, the probability density measure $\mathrm{d}F(\boldsymbol{\xi})$ can be written as

$$\mathrm{d}F(\boldsymbol{\xi}) = (2\pi)^{-\eta/2}\exp\left(-\tfrac{1}{2}\boldsymbol{\xi}^{\mathrm{T}}\boldsymbol{\xi}\right)\mathrm{d}\boldsymbol{\xi}. \tag{12}$$

The original Wiener-polynomial chaos has been successfully used in solving several stochastic PDEs with Gaussian inputs and some stochastic PDEs with allied non-Gaussian inputs (e.g. log-Normal) [8,10–13]. However, in general for non-Gaussian inputs, the optimal exponential convergence rate will not be realized. Karniadakis and coworkers [15] found that the rate of convergence severely deteriorates in some cases. Thus, in this work, we choose the basis from the broad Askey scheme of orthogonal polynomials. This helps in selecting optimal bases for a wide variety of non-Gaussian inputs. The generalized polynomial chaos expansion for $X(\omega)$ can be written as follows [14]:

$$(\omega) = \ {}_0 I_0 + \sum_{_1=1}^{\eta} \ {}_1 I_1(\zeta_{\ _1}(\omega)) + \cdots + \sum_{_1=1}^{\eta} \cdots \sum_{_\eta=1}^{\eta-1} \ {}_{1\,2\cdots\eta} I_{\eta}\,(\zeta_{\ _1}(\omega), \ldots, \zeta_{\ _\eta}(\omega)) + \cdots \tag{13}$$

where $I_n(\zeta_{i_1}(\omega),\ldots,\zeta_{i_n}(\omega))$ denotes the Wiener–Askey polynomial chaos of order n in terms of the uncorrelated random vector $\boldsymbol{\zeta} = (\zeta_1(\omega),\ldots,\zeta_n(\omega))$. Again, for notational convenience we write

$$(\omega) = \sum_{_\iota=0}^{\infty} \hat{}_\iota \, \psi_{_\iota}\,(\boldsymbol{\zeta}), \tag{14}$$

where $\psi_j(\boldsymbol{\zeta})$ here has a one-to-one relationship with an Askey polynomial $I_n(\zeta_{i_1},\ldots,\zeta_{i_n})$.

It can be shown by generalizing the Cameron and Martin theorem that this expansion converges to any second-order random variable in the L_2 sense [9]. Table 1 provides classes of Askey polynomials that have the same weighting function as certain kind of distributions [35].

3. The stochastic advection–diffusion problem

Let $\mathscr{D} \subset \mathbb{R}$, where $d \geqslant 1$ is the number of space dimensions, be an open, bounded, polyhedral domain with piecewise smooth boundary $\Gamma, \mathscr{T} = \{ \ : \ \in [0, \ ]\}$ and $(\Omega, \mathscr{F}, \mathscr{P})$ be a probability space. $\mathscr{T}$ is identified as the time interval for simulation.

The transient advection and diffusion of a stochastic scalar process in the presence of a divergence-free stochastic velocity field $\mathbf{a}(\mathbf{x},\omega)$ in a medium with random non-negative diffusion coefficient $v(\omega)$ can be defined as follows.

Find $\phi(\mathbf{x}, \ ,\omega) : (\mathscr{D} \times \mathscr{T} \times \Omega) \mapsto \mathbb{R}$ such that:

$$\partial\, \phi + \mathscr{L}\phi = \dot{} \ , \qquad (\mathbf{x}, \ ,\omega) \in (\mathscr{D} \times \mathscr{T} \times \Omega), \tag{15}$$

$$\phi(\mathbf{x}, \ ,\omega) = {}_{f} \ (\mathbf{x}, \ ,\omega), \quad (\mathbf{x}, \ ,\omega) \in (\Gamma \times \mathscr{T} \times \Omega), \tag{16}$$

$$\phi(\mathbf{x}, 0, \omega) = \phi_0(\mathbf{x}, \omega), \quad (\mathbf{x}, \omega) \in (\mathscr{D} \times \Omega), \tag{17}$$

where $\mathscr{L}\phi(\mathbf{x}, \ ,\omega)$ is the stochastic advective–diffusive operator defined as

$$\mathscr{L}\phi(\mathbf{x}, \ ,\omega) = \mathbf{a} \cdot \nabla\phi - \nabla \cdot (v \nabla\phi). \tag{18}$$

Table 1
Orthogonal polynomials from Askey series with associated random variables [35]

Random variable	Askey chaos	Support space
Gaussian	Hermite-polynomials	$(-\infty,\infty)$
Uniform	Legendre-polynomials	$[-1,1]$
Beta	Jacobi-polynomials	$[a,b]$
Gamma	Laguerre-polynomials	$[0,\infty)$

. $(\mathbf{x},\ ,\omega) : (\mathscr{D}\times\mathscr{T}\times\Omega)\mapsto\mathbb{R}$ is a source term and $_f\ (\mathbf{x},\ ,\omega) : (\Gamma\times\mathscr{T}\times\Omega)\mapsto\mathbb{R}$ is the specified stochastic Dirichlet boundary condition.

It should be emphasized here that the probability model used for the advection velocity $\mathbf{a}(\mathbf{x},\omega)$ should ensure the divergence-free constraint $\nabla\cdot\mathbf{a}=0$ and the probability model used for the diffusion coefficient $v(\omega)$ should have a non-negative support space.

Since Gaussian distribution assigns finite probability to negative values, the diffusion coefficient cannot be modeled as a Gaussian random variable. This startling result has been proved for the case of diffusion problems [36] wherein, it was shown that a Gaussian thermal conductivity assumption leads to an ill-posed polynomial chaos system of equations when implemented using the spectral stochastic finite element method.

The argument ω shall henceforth be dropped if it is clear by the content that the quantities are random.

3.1. Variational formulation

Let $\mathscr{U}$ denote the trial solution space and $\mathscr{V}$ denote the weighting function space. $\mathscr{U}$ and $\mathscr{V}$ are defined as follows:

$$\mathscr{U}=\{\ :\ (\mathbf{x},\ ,\omega)\in H^1(\mathscr{D})\times L_2(\mathscr{T})\times L_2(\Omega),\quad\ =\ _f\ \text{ on }\Gamma\},\tag{19}$$

$$\mathscr{V}=\{\ :\ (\mathbf{x},\omega)\in H^1(\mathscr{D})\times L_2(\Omega),\qquad=0\text{ on }\Gamma\},\tag{20}$$

where $L_2(\Omega)$ denotes the space of second order random variables, $L_2(\mathscr{T})$ denotes the space of square integrable functions defined on the time interval $\mathscr{T}$ and $H^1(\mathscr{D})$ is the Sobolev space of square-integrable functions with square-integrable derivatives defined on the spatial domain $\mathscr{D}$.

The variational counterpart of the strong system of Eqs. (15)–(17) reads as follows.

Find $\phi\in\mathscr{U}$ such that $\forall\ \in\mathscr{V}$ and $\forall\ \in\mathscr{T}$

$$(\partial\ \phi,\ \ )+a(\phi,\ \ )=(.\ ,\ \ ).\tag{21}$$

The bilinear form $b(\phi,w)$ introduced above is given by

$$a(\phi,\ \ )=(\mathscr{L}\phi,\ \ )=(\phi,\mathscr{L}^*\ \ )=(\mathbf{a}\cdot\nabla\phi,\ \ )+(v\nabla\phi,\nabla\ \ )_{\mathrm{v}},\tag{22}$$

where the inner-product $(\mathbf{g},\mathbf{h})_{\mathrm{v}}$ is defined as

$$(\mathbf{g},\mathbf{h})_{\mathrm{v}}=\int_{\mathscr{D}}E[\mathbf{g}(\mathbf{x},\ ,\omega)\cdot\mathbf{h}(\mathbf{x},\ ,\omega)]\mathrm{d}\mathbf{x}=\int_{\mathscr{D}}\int_{\Omega}\mathbf{g}(\mathbf{x},\ ,\omega)\cdot\mathbf{h}(\mathbf{x},\ ,\omega)\,\mathrm{d}\mathscr{P}\,\mathrm{d}\mathbf{x}\tag{23}$$

and the inner-product (g,h) for a given $\in\mathscr{T}$ is defined as

$$(_f\ ,_g)=\int_{\mathscr{D}}E[_f\ (\mathbf{x},\ ,\omega)_g(\mathbf{x},\ ,\omega)]\mathrm{d}\mathbf{x}=\int_{\mathscr{D}}\int_{\Omega_f}\ (\mathbf{x},\ ,\omega)_g(\mathbf{x},\ ,\omega)\,\mathrm{d}\mathscr{P}\,\mathrm{d}\mathbf{x}.\tag{24}$$

It should be noted that the first two equalities in Eq. (22) require stronger regularity conditions (differentiability) on the solution $\phi(\mathbf{x},t,\omega)$. The assumption that $g(\mathbf{x},t,\omega)$ and $h(\mathbf{x},t,\omega)$ are second order random processes together with the Schwarz inequality

$$E[_f\ (\mathbf{x},\ ,\omega)_g(\mathbf{x},\ ,\omega)]\leqslant(E\,|_f\ (\mathbf{x},\ ,\omega)|^2)^{1/2}(E\,|_g(\mathbf{x},\ ,\omega)|^2)^{1/2}<\infty\tag{25}$$

guarantee that the inner-product in Eq. (24) is finite.

3.2. Variational multiscale method

Let $\phi = \bar{\phi} + \phi'$ be an overlapping sum decomposition of the exact solution $\phi(\mathbf{x},t,\omega)$, where $\bar{\phi}$ represents the contribution due to resolved large scales and ϕ' is the contribution due to unresolved small scales. The small scales will henceforth be referred to as subgrid scales [21,22,24,25]. Similar decomposition is considered for the weighting function $= ^{-} + ^{\prime}$.

Let $\mathscr{U} = \bar{\mathscr{U}} \oplus \mathscr{U}'$ and $\mathscr{V} = \bar{\mathscr{V}} \oplus \mathscr{V}'$, where $\bar{\mathscr{U}}$ and $\mathscr{U}'$ represent the large and subgrid scale function spaces for the solution and let $\bar{\mathscr{V}}$ and $\mathscr{V}'$ represent the large and subgrid scales for the weighting function. We further assume

$$\bar{\phi} = _{f} \quad \forall \bar{\phi} \in \bar{\mathscr{U}},\ \mathbf{x} \in \Gamma, \tag{26}$$

$$\phi' = 0 \quad \forall \phi' \in \mathscr{U}',\ \mathbf{x} \in \Gamma, \tag{27}$$

$$^{-} = 0 \quad \forall ^{-} \in \bar{\mathscr{V}},\ \mathbf{x} \in \Gamma, \tag{28}$$

$$^{\prime} = 0 \quad \forall \ ^{\prime} \in \mathscr{V}',\ \mathbf{x} \in \Gamma. \tag{29}$$

The objective of the variational multiscale (VMS) method is to derive a variational statement for $\bar{\phi}$ that takes into account an approximate model for the subgrid scale solution ϕ'.

Typically, the large scale trial solution and weighting function spaces are associated with finite element spaces and hence are finite-dimensional. In contrast, the subgrid scale function spaces do not possess scaling information and are infinite-dimensional.

Using the multiscale framework developed above, Eq. (21) can be split into two-scale problems as follows:

$$(\partial \bar{\phi} + \partial \phi', ^{-}) + a(\bar{\phi}, ^{-}) + a(\phi', ^{-}) = (. , ^{-}), \tag{30}$$

$$(\partial \bar{\phi} + \partial \phi', \ ^{\prime}) + a(\bar{\phi}, \ ^{\prime}) + a(\phi', \ ^{\prime}) = (. , \ ^{\prime}). \tag{31}$$

The main idea here is to use Eq. (31) to arrive at approximate model for $\phi'(\mathbf{x},t,\omega)$. This approximate model is then used to eliminate ϕ' from Eq. (30).

Until now, Eqs. (30) and (31) are exact, highly coupled and hence extremely tough to solve. Thus, several stages of modeling assumptions are introduced to simplify the subgrid scale Eq. (31).

Assumption 1. The subgrid scales are quasi-static, i.e., $\partial_t \phi' \approx 0$. The validity of this assumption is discussed in [37–39]. This assumption requires that the time integration be accurate enough so that the large scale can capture the temporal variation of the solution. In problems involving high Reynolds number flows, one needs to explicitly track the subscales [40–42]. Since this preliminary effort is to integrate the variational multiscale method with the stochastic finite element method and to study the effects of stochastic modeling on the stabilization parameters, only quasistatic subgrid scales are investigated herein.

Eq. (31) can now be simplified as

$$a(\phi', \ ^{\prime}) = (. \ - \partial \bar{\phi}, \ ^{\prime}) - a(\bar{\phi}, \ ^{\prime}). \tag{32}$$

The above equation together with strong regularity conditions for ϕ (see Eq. (22)) yields the following subgrid scale equation.

For $\phi' \in \mathscr{U}'$, the following is satisfied for all $^{\prime} \in \mathscr{V}'$

$$(\mathscr{L}\phi', \ ^{\prime}) = (\mathscr{R}\bar{\phi}, \ ^{\prime}), \tag{33}$$

where $\mathscr{R}\bar{\phi}(\mathbf{x}, \ ,\omega) = . \ - \partial \bar{\phi} - \mathscr{L}\bar{\phi}$ is the large scale residual.

Consider a finite element partition into elements indexed as $\mathscr{E} = \{1, \ldots, \mathrm{Nel}\}$, dividing the spatial domain $\mathscr{D}$ into subdomains $\mathscr{D}^{(e)}$ with element boundaries $\Gamma^{(e)}$. The strong form of Eq. (33) is then approximated over each element (e) as follows:

$$\mathscr{L}\phi' = \mathscr{R}\bar{\phi}, \quad (\mathbf{x}, \, , \omega) \in (\mathscr{D}^{(e)} \times \mathscr{T} \times \Omega), \tag{34}$$

$$\phi' = 0, \quad (\mathbf{x}, \, , \omega) \in (\Gamma^{(e)} \times \mathscr{T} \times \Omega). \tag{35}$$

The assumption that the subgrid scale solution vanishes at element boundaries is a strong assumption and is intimately linked with the idea of residual-free bubble functions [23,43]. For computational simplicity, it is desirable to derive an approximate algebraic model for the subgrid scale solution. This leads to the second modeling assumption.

Assumption 2. The algebraic subgrid scale model is considered to be of the form

$$\phi'(\mathbf{x}, \, , \omega) \approx \tau(\mathbf{x}, \omega)\mathscr{R}\bar{\phi}(\mathbf{x}, \, , \omega), \tag{36}$$

where the parameter $\tau(\mathbf{x},\omega)$ is inherently stochastic and is interpreted as the intrinsic time scale for the stochastic subgrid solution.

With substitution of Eq. (36) into Eq. (30), the complete multiscale stabilized variational statement for the stochastic advection–diffusion problem can be written as

$$\begin{aligned}
&(\partial \bar{\phi} + \mathbf{a} \cdot \nabla\bar{\phi}, {}^{-} + \tau(\mathbf{x}, \omega)[\mathbf{a} \cdot \nabla^{-} + v(\omega)\Delta^{-}]) + (v(\omega)\nabla\bar{\phi}, \nabla^{-})_{\mathrm{v}} \\
&\quad - (v(\omega)\Delta\bar{\phi}, \tau(\mathbf{x}, \omega)[\mathbf{a} \cdot \nabla^{-} + v(\omega)\Delta^{-}]) \\
&\quad = (. \, , {}^{-} + \tau(\mathbf{x}, \omega)[\mathbf{a} \cdot \nabla^{-} + v(\omega)\Delta^{-}]),
\end{aligned} \tag{37}$$

where Δ denotes the Laplacian operator ∇^2. Typically for linear finite elements most of the terms in the above stabilized formulation drop out leading to a SUPG like formulation for stochastic advection–diffusion equation.

We shall now proceed to derive models for the intrinsic subgrid time scale. For simplicity, in the ensuing derivation it will be assumed that the advection velocity is constant in an element. The results however are general and can be used for velocity and diffusion coefficient varying within an element.

3.3. Models for τ-intrinsic subgrid time scale

Models for the intrinsic subgrid time scale are not unique. Different models can be suggested based on the level of subgrid characterization desired, phase lag and transient behavior restrictions. All these models, however, should essentially possess similar behavior in the limits of pure advection and pure diffusion.

Several techniques such as Green's function methods, Fourier analysis, Taylor series expansion can be employed to arrive at different models for τ. In this work however, we follow the Fourier analysis approach. This helps keep the derivation of τ consistent for the stochastic advection–diffusion and stochastic Navier–Stokes problems.

We begin by introducing the Fourier transform of a generic stochastic function $g(\mathbf{x},\omega)$ defined on an element (e)

$$\hat{f}(\mathbf{k}, \omega) := \int_{\mathscr{D}^{(e)}} \exp\left(-\mathrm{i}\frac{\mathbf{k} \cdot \mathbf{x}}{h}\right) f(\mathbf{x}, \omega) \, \mathrm{d}\mathbf{x}, \tag{38}$$

where h is an elemental length parameter, $\mathbf{k}$ denotes the wave number and ω denotes association with the probability space.

In the definition of variational multiscale framework, we interpreted the exact solution as an overlapping sum of a resolved large scale component and an unresolvable subgrid scale component. Thus in the wave number space, the large scale soluton corresponds to the lower wave number modes and the subgrid scale solution corresponds to the larger wave number modes. This allows us to arrive at an approximation for the spatial derivative of the generic stochastic function $g(\mathbf{x},\omega)$

$$\frac{\hat{\partial}}{\partial_{x_j}}(\mathbf{k},\omega) = \int_{\Gamma^{(e)}} n_j \exp\left(-\mathrm{i}\frac{\mathbf{k}\cdot\mathbf{x}}{h}\right) g(\mathbf{x},\omega)\,\mathrm{d}\Gamma + \mathrm{i}\frac{k_j}{h}\hat{g}(\mathbf{k},\omega) \approx \mathrm{i}\frac{k_j}{h}\hat{g}(\mathbf{k},\omega), \tag{39}$$

where n_j is the jth component of the outward unit normal to the element (e). The Fourier transform of the subgrid scale Eq. (34) now yields

$$\hat{\phi}'(\mathbf{k},\,,\omega) \approx \hat{\tau}(\mathbf{k},\omega)\hat{\mathscr{R}}\hat{\bar{\phi}}(\mathbf{k},\,,\omega), \quad \hat{\tau}(\mathbf{k},\omega) := \left(\nu(\omega)\frac{|\,\mathbf{k}|^2}{h^2} + \mathrm{i}\frac{\mathbf{k}\cdot\mathbf{a}}{h}\right)^{-1}. \tag{40}$$

Note that in the above expression the assumption of velocity being constant within an element is required. Using Plancheral's formula and the mean value theorem, we arrive at [38]

$$\tau(\omega) \approx \left[\left(c_1(\omega)\frac{\nu(\omega)}{h^2}\right)^2 + \left(c_2(\omega)\frac{|\,\mathbf{a}\,|}{h}\right)^2\right]^{-1/2}, \tag{41}$$

where $|\mathbf{a}| = |\mathbf{a}(\omega)|$ is defined as

$$|\,\mathbf{a}\,| = |\,\mathbf{a}(\omega)\,| = \sqrt{\mathbf{a}\cdot\mathbf{a}}. \tag{42}$$

This choice of the intrinsic time scale makes $\tau(\omega)\mathscr{R}\bar{\phi}$ equal to the subgrid solution ϕ' in the L_2 sense.

Furthermore, the asymptotic behavior of τ in the diffusive limit is dominated by the term $h^2/\nu(\omega)$ and the asymptotic behavior in the advection limit is dominated by the term $h/|\mathbf{a}|$. The intimate link between Eq. (41) and SUPG-like stabilization methods is seen by choosing the random constants as $c_1(\omega) = 4$ and $c_2(\omega) = 2$. This leads to an intrinsic subgrid time scale model of the form

$$\tau(\omega) \approx \left[\left(4\frac{\nu(\omega)}{h^2}\right)^2 + \left(2\frac{|\,\mathbf{a}\,|}{h}\right)^2\right]^{-1/2}. \tag{43}$$

In this work, however, we chose a model having similar asymptotic properties as the model in Eq. (43). The proposed model minimizes phase lag in transient problems and extends to the more general case of spatially varying stochastic velocity field and random diffusion coefficient. It is given as

$$\tau(\mathbf{x},\omega) = \frac{h}{2\,|\,\mathbf{a}(\mathbf{x},\omega)\,|}\cdot\,(\mathrm{Pe}(\mathbf{x},\omega)), \tag{44}$$

where h is the elemental length and the function $f(\mathrm{Pe})$ is defined for linear finite elements as

$$\cdot\,(\mathrm{Pe}) = \frac{\mathrm{Pe}}{3}\mathbb{I}_{[\mathrm{Pe}:0<\mathrm{Pe}\leqslant 3]}(\mathrm{Pe}) + \mathbb{I}_{[\mathrm{Pe}:\mathrm{Pe}>3]}(\mathrm{Pe}), \tag{45}$$

where $\mathbb{I}_A(\mathbf{x})$ is the indicator function for set $\{A\}$ and Pe is the element Pèclet number

$$\mathrm{Pe}(\mathbf{x},\omega) = \frac{|\,\mathbf{a}(\mathbf{x},\omega)\,|\,h}{2\nu(\omega)}. \tag{46}$$

Remark 1. $\tau(\mathbf{x},\omega)$ represents the intrinsic time scale for a real process via the subgrid solution. Hence the model chosen for τ should ensure that the subgrid scale solution has finite statistical moments (mean and variance). However, the statistical behavior of τ depends on the kind of probability models chosen for the advection velocity and diffusion coefficient.

Given a model for $\tau(\mathbf{x},\omega)$, the above conditions constrain the probability models available for $\mathbf{a}(\mathbf{x},\omega)$ and $\nu(\omega)$. Typically, spurious oscillations are noticed in the numerical solution when probability models with unbounded support space are specified for the advection velocity and diffusion coefficient. The models that fall under this category are normal, gamma and lognormal distribution models. Most probability models with finite support space are usually compatible with the proposed intrinsic time scale model. These include beta and uniform probability models.

We shall now elaborate on the remark using a simple one-dimensional advection–diffusion case study.

3.4. Intrinsic time scale models and induced constraints – a one-dimensional case study

Consider the one-dimensional version of the stochastic convection-diffusion problem defined by Eqs. (15)–(17) with the spatial domain $\mathscr{D} = [0, L]$. The norm of the advection velocity then simply is $|a|$, the absolute value of $a(\mathbf{x},\omega)$. We do not use boldface for the advection velocity since it has a single component. The intrinsic subgrid time scale τ for this problem is as defined in Eq. (44). We now consider different probability models for advection velocity and diffusion coefficient and analyze the behavior of the subgrid scale solution.

3.4.1. Case I: Pure advection, no source term

In this case, the expression for τ simplifies to

$$\tau(\cdot,\omega) = \frac{h}{2\,|\mathbf{a}(\cdot,\omega)|} \tag{47}$$

and the subgrid scale solution can be written as

$$\phi'(\cdot,\omega) = -\frac{h}{2\,|\mathbf{a}(\cdot,\omega)|}\left(\partial\,\bar{\phi} + \frac{\partial\bar{\phi}}{\partial_{\cdot}}\right). \tag{48}$$

Since, ϕ' represents the subgrid scale for a physical quantity, the statistical moments for ϕ' upto second order should be finite [since $\phi' \in H^1(\mathscr{D}) \times L_2(\mathscr{T}) \times L_2(\Omega)$].

Expanding $\bar{\phi}$ in a truncated generalized polynomial chaos expansion, we obtain the following:

$$\phi'(\cdot,\omega) = -\sum_{=0}^{P} \frac{h}{2\,|\mathbf{a}(\cdot,\omega)|}\left(\partial\,\bar{\phi}\,\psi\,(\omega) + \frac{\partial\bar{\phi}\,\psi\,(\omega)}{\partial_{\cdot}}\right), \tag{49}$$

where the polynomials $\{\psi\,(\omega)\}_{=0}^{P}$ belong to the Askey series of orthogonal polynomials and form an orthogonal basis of $L_2(\Omega)$.

If we consider the advection velocity to be a normal random variable with $N(\mu,\sigma)$ distribution, the mean of ϕ' can be written as

$$E\phi' = -\int_{-\infty}^{\infty}\sum_{=0}^{P}\frac{h}{2\,|\mu+\sigma\xi|}\left(\partial\,\bar{\phi}\,\psi\,(\xi) + \frac{\partial\bar{\phi}\,\psi\,(\xi)}{\partial_{\cdot}}\right)\frac{1}{\sqrt{2\pi}}\exp\left(-\frac{1}{2}\xi^2\right)\mathrm{d}\xi. \tag{50}$$

Note that, in the above equations, ω dependence is shown via ξ and that all polynomial chaoses are functions of ξ (here Hermite polynomials).

In order for the above integral to converge, it can be shown that the following term needs to be finite (note that the coefficients of polynomial chaos $\bar{\phi}_0, \bar{\phi}_1, \ldots$ are deterministic):

$$\int_{-\infty}^{\infty} \frac{\delta}{2 \mid \mu + \sigma\xi \mid} \left(\partial \bar{\phi}_0 + \mu \frac{\partial \bar{\phi}_0}{\partial \_} \right) \frac{1}{\sqrt{2\pi}} \exp\left(-\frac{1}{2}\xi^2 \right) \mathrm{d}\xi. \tag{51}$$

However, the behavior of the above integral is governed by the divergent integral

$$\int_{-\infty}^{\infty} \frac{1}{2 \mid \mu + \sigma\xi \mid} \frac{1}{\sqrt{2\pi}} \exp\left(-\frac{1}{2}\xi^2 \right) \mathrm{d}\xi. \tag{52}$$

Hence, a normal distribution is not an appropriate model for the advection velocity under the proposed choice of τ. However, if a uniform distribution model is chosen for a with

$$= \gamma + \delta\zeta(\omega), \quad \zeta \overset{\mathrm{d}}{=} \quad [-1, 1], \quad \gamma,\ \delta > 0,\ \delta < \gamma, \tag{53}$$

then it can be shown that the first two statistical moments of ϕ' are finite. The exact expressions are very complicated and hence are not supplied here. However, the counterpart of Eq. (51) can be written as

$$\int_{\gamma-\delta}^{\gamma+\delta} \frac{\delta}{2 \mid \quad \mid} \left(\partial \bar{\phi}_0 + \mu \frac{\partial \bar{\phi}_0}{\partial \_} \right) \frac{1}{2\delta} \mathrm{d} \ . \tag{54}$$

This integral converges and has the value

$$\left(\partial \bar{\phi}_0 + \mu \frac{\partial \bar{\phi}_0}{\partial \_} \right) \{ \log(\gamma + \delta) - \log(\gamma - \delta) \} \frac{1}{2\delta}. \tag{55}$$

Most probability distributions with finite support behave in a similar manner under the proposed assumption of τ. This case study is not to discourage the use of probability distributions with infinite support. The study is to point to the fact that caution has to be exerted to ensure that the model for τ and the input uncertainty models are compatible.

3.4.2. Case II: Diffusion dominant regime, no source term

In this case, the expression for τ simplifies to

$$\tau(\omega) = \frac{\delta^2}{4\nu(\omega)}. \tag{56}$$

Analysis of the behavior of ϕ' for this case proceeds along similar lines as in the previous case. In this case, even distributions with infinite support like Gamma, χ^2 and shifted log-normal ensure $\phi' \in L_2(\Omega)$.

However, one should be careful in selecting distributions with infinite support. Choosing $\nu(\omega)$ to be of the form $|X(\omega)|$ where $(\omega) \overset{\mathrm{d}}{=} N(\mu, \sigma)$, leads to problems very similar to the previous case. This is because $|X(\omega)|$ attributes non vanishing probability for values near zero. Since $\nu(\omega)^{-1}$ is unbounded near $\nu = 0$, the expectation diverges. This leads to an important observation summarized below.

Remark 2. The selection of distributions for advection velocity and diffusion coefficient is constrained upon the definition of the intrinsic time scale. There is a great scope for defining appropriate models for τ that are consistent with the probability models for **a** and ν.

4. The stochastic incompressible Navier–Stokes equations

Let $\mathscr{D} \subset \mathbb{R}$, where $d \geqslant 1$ is the number of space dimensions, be an open, bounded domain with piecewise smooth boundary $\Gamma, \mathscr{T} = \{ \; : \; \in [0, \;]\}$ be the time interval of analysis and $(\Omega, \mathscr{F}, \mathscr{P})$ be a probability space.

The strong form of stochastic Navier–Stokes problem consists of finding the stochastic velocity $\boldsymbol{v}(\mathbf{x},t,\omega)$ and pressure $p(\mathbf{x},t,\omega)$ such that

$$\partial \; + \; \cdot \nabla \; - v(\omega)\Delta \; + \nabla \; = \, . \, (\mathbf{x}, \; , \omega), \quad (\mathbf{x}, \; , \omega) \in (\mathscr{D} \times \mathscr{T} \times \Omega), \tag{57}$$

$$\nabla \cdot \; = 0, \quad (\mathbf{x}, \; , \omega) \in (\mathscr{D} \times \mathscr{T} \times \Omega), \tag{58}$$

$$= \, _{f} \, (\mathbf{x}, \; , \omega), \quad (\mathbf{x}, \; , \omega) \in (\Gamma \times \mathscr{T} \times \Omega), \tag{59}$$

$$(\mathbf{x}, 0, \omega) = \; _{0}(\mathbf{x}, \omega), \quad (\mathbf{x}, \omega) \in (\mathscr{D} \times \Omega), \tag{60}$$

where Δ denotes the Laplacian operator ∇^2, $v(\omega)$ is the random kinematic viscosity and $f(\mathbf{x},t,\omega)$ is a stochastic forcing term. The uncertainty in this problem comes from $v(\omega)$, $f(\mathbf{x},t,\omega)$, initial and boundary conditions. In this work, we consider constant property flows, hence the kinematic viscosity is considered to be a random variable with a non-negative support space (regions of strictly positive probability density).

4.1. Variational formulation

Let $\mathscr{U}$ and $\mathscr{V}$, the trial solution and weighting function spaces for velocity and let $\mathscr{X}$ and $\mathscr{X}_0$ denote the trial and weighting function spaces for pressure:

$$\mathscr{U} = \{ \; : \; (\mathbf{x}, \; , \omega) \in [H^1(\mathscr{D}) \times L_2(\mathscr{T}) \times L_2(\Omega)]^{\mathrm{d}}, \quad = \, _{f} \; \text{ on } \Gamma\}, \tag{61}$$

$$\mathscr{V} = \{ \; : \; (\mathbf{x}, \omega) \in [H^1(\mathscr{D}) \times L_2(\Omega)]^{\mathrm{d}}, \quad = 0 \text{ on } \Gamma\}, \tag{62}$$

$$\mathscr{X} = \{ \; : \; (\mathbf{x}, \; , \omega) \in L_2(\mathscr{D}) \times L_1(\mathscr{T}) \times L_2(\Omega)\}, \tag{63}$$

$$\mathscr{X}_0 = \{ \; : \; (\mathbf{x}, \omega) \in L_2(\mathscr{D}) \times L_2(\Omega)\}, \tag{64}$$

where $L_1(\mathscr{T})$ denotes functions of bounded variation in time. It should be noted here that the function spaces used for velocity and pressure do not have the same regularity conditions (velocity should be twice differentiable whereas pressure need only be once differentiable), hence the weighting function spaces also differ.

The variational formulation counterpart for the strong system of Eqs. (57) and (58) reads as follows. Find $(\; , \;) \in (\mathscr{U}, \mathscr{X})$ such that $\forall (\; , \;) \in (\mathscr{V}, \mathscr{X}_0)$, the following is satisfied $\forall \; \in \mathscr{T}$

$$(\partial \; , \;) + (v(\omega)\nabla \; , \nabla \;)_{\mathrm{v}} + (\; \cdot \nabla \; , \;) - (\; , \nabla \cdot \;) = (. \; , \;), \tag{65}$$

$$(\; , \nabla \cdot \;) = 0, \tag{66}$$

where the inner-product $(\mathbf{g},\mathbf{h})$ is here defined as

$$(\mathbf{g}, \mathbf{h}) := \int_{\mathscr{D}} E[\mathbf{g} \cdot \mathbf{h}] \, \mathrm{d}\mathbf{x} \tag{67}$$

and the inner-product $(\mathbf{g},\mathbf{h})_{\mathrm{v}}$ is defined as

$$(\mathbf{g}, \mathbf{h})_{\mathrm{v}} := \int_{\mathscr{D}} E[\mathbf{g} : \mathbf{h}] \, \mathrm{d}\mathbf{x}. \tag{68}$$

It is assumed that the initial condition is satisfied in a weak sense.

4.2. Variational multiscale hypothesis

Consider an overlapping sum decomposition for velocity and pressure $= ^{-} + ^{\prime}$ and $= ^{-} + ^{\prime}$. Consider similar decomposition for the weighting functions $= ^{-} + ^{\prime}$ and $= ^{-} + ^{\prime}$. This induces a multiscale decomposition for the function spaces of the form $\mathcal{U} = \bar{\mathcal{U}} \oplus \mathcal{U}'$, $\mathcal{V} = \bar{\mathcal{V}} \oplus \mathcal{V}'$, $\mathcal{X} = \bar{\mathcal{X}} \oplus \mathcal{X}'$ and $\mathcal{X}_0 = \bar{\mathcal{X}}_0 \oplus \mathcal{X}'_0$, where the bar indicates reference to large resolved scales and the dash indicates reference to the subgrid scales.

Unlike the stochastic advection–diffusion equation, the presence of a nolinear convection term necessitates an apriori assumption in the derivation of a multiscale stabilized formulation.

Assumption 3. Assuming the large scales are sufficiently resolved, the subgrid scale solution can be considered to be small compared to the resolved large scale solution. This justifies a one step Picard's linearization for the nonlinear advection term

$$\cdot \nabla \approx ^{-} \cdot \nabla ^{\prime} + ^{-} \cdot \nabla ^{-}. \tag{69}$$

This assumption is valid for low to moderate Reynolds numbers.

At high Reynolds numbers, adequate grid resolution is computationally highly demanding. Hence often the large scales are only partially resolved. As a consequence, the kinetic energy held in subgrid scales becomes substantial (>20% of energy in the system). Further, the nonlinear subgrid convection term $\boldsymbol{v}' \cdot \nabla \boldsymbol{v}'$ assumes importance. Thus, a coupled subgrid scale and resolved scale equation has to be solved at each time step. Hence such high Reynolds number flows are not addressed in this preliminary work.

The variational form given by Eqs. (65) and (66) now reads as follows:

$$(\partial ^{-} + \partial ^{\prime}, ^{-}) + (\nu \nabla ^{-} + \nu \nabla ^{\prime}, \nabla ^{-})_{\mathrm{v}} + (^{-} \cdot \nabla ^{-} + ^{-} \cdot \nabla ^{\prime}, ^{-}) - (^{-} + ^{\prime}, \nabla \cdot ^{-}) = (. , ^{-}), \tag{70}$$

$$(\nabla \cdot ^{-} + \nabla \cdot ^{\prime}, ^{-}) = 0, \tag{71}$$

$$(\partial ^{-} + \partial ^{\prime}, ^{\prime}) + (\nu \nabla ^{-} + \nu \nabla ^{\prime}, \nabla ^{\prime})_{\mathrm{v}} + (^{-} \cdot \nabla ^{-} + ^{-} \cdot \nabla ^{\prime}, ^{\prime}) - (^{-} + ^{\prime}, \nabla \cdot ^{\prime}) = (. , ^{\prime}), \tag{72}$$

$$(\nabla \cdot ^{-} + \nabla \cdot ^{\prime}, ^{\prime}) = 0. \tag{73}$$

Assumption 4. Consider subgrid scale velocity and pressure to be quasistatic random processes $\partial_t v' \approx 0$ and $\partial_t p' \approx 0$ [37,38]. If the time scales of subgrid solutions are different from those of the large scale solutions as in the case of turbulent flows, this assumption is not valid. We would then need to explicitly track the subscale evolution in time. By assuming linearity of subscales, we tacitly assume that the time scales of subgrid solution and large scale are nearly the same and that we capture the complete time evolution of the solution through $\partial ^{-}$. Further, the following relations hold under assumption of stronger regularity conditions on velocity and pressure (twice differentiability).

The subgrid scale variational form given by Eqs. (72) and (73) yield the following strong system of subgrid scale equations:

$$^{-} \cdot \nabla ^{\prime} - \nu \Delta ^{\prime} + \nabla ^{\prime} = \mathscr{R}_{\mathrm{m}}(^{-}, ^{-}), \tag{74}$$

$$\nabla \cdot ^{\prime} = \mathscr{R}_{\mathrm{c}}(^{-}), \tag{75}$$

where Δ denotes the Laplacian operator and $\mathscr{R}_{\mathrm{m}}(^{-}, ^{-})$ and $\mathscr{R}_{\mathrm{c}}(^{-})$ are the momentum and continuity equation residuals for the large resolved scales given as follows:

$$\mathscr{R}_{\mathrm{m}}(\bar{\ },\bar{\ }) = \dot{\ } - \partial\bar{\ } - \bar{\ }\cdot\nabla\bar{\ } + \nu\Delta\bar{\ } - \nabla\bar{\ }, \tag{76}$$

$$\mathscr{R}_{\mathrm{c}}(\bar{\ }) = -\nabla\cdot\bar{\ }. \tag{77}$$

Note that the pressure does not directly affect the residual of the continuity equation. Without loss of generality it can be assumed that the large scale momentum residual is divergence free. As in the case of stochastic advection–diffusion equation, the behavior of subgrid scale solutions will be neglected on element boundaries. Further, it will be assumed for the time scale calculations that the velocity field within an element is constant. This assumption is to simplify the derivation and can be relaxed.

Now, considering the Fourier transform of the subgrid scale Eqs. (74) and (75), we obtain:

$$\left(\nu\frac{|\mathbf{k}|^2}{g^2} + \mathrm{i}\frac{\bar{\ }\cdot\mathbf{k}}{g}\right)\hat{\ }'(\mathbf{k},\ ,\omega) + \mathrm{i}\frac{\mathbf{k}}{g}\hat{\ }'(\mathbf{k},\ ,\omega) = \hat{\mathscr{R}}_{\mathrm{m}}, \tag{78}$$

$$\mathrm{i}\frac{\mathbf{k}}{g}\cdot\hat{\ }'(\mathbf{k},\ ,\omega) = \hat{\mathscr{R}}_{\mathrm{c}}. \tag{79}$$

Noting that the large scale residual is divergence-free and taking inner product of Eq. (78) with i(**k**/*h*) (the divergence operator in wave-number space), results in the following:

$$\left(\nu\frac{|\mathbf{k}|^2}{g^2} + \mathrm{i}\frac{\bar{\ }\cdot\mathbf{k}}{g}\right)\hat{\mathscr{R}}_{\mathrm{c}} - \frac{|\mathbf{k}|^2}{g^2}\hat{\ }(\mathbf{k},\ ,\omega) = 0. \tag{80}$$

Using an approach similar to the stochastic advection–diffusion equation and by using Plancheral's formula and mean value theorem, we arrive at the subgrid scale models:

$$'(\mathbf{x},\ ,\omega) \approx \tau_{(\ )}(\mathbf{x},\omega)\mathscr{R}_{\mathrm{m}}(\bar{\ },\bar{\ }), \tag{81}$$

$$'(\mathbf{x},\ ,\omega) \approx \tau_{(\ )}(\mathbf{x},\omega)\mathscr{R}_{\mathrm{c}}(\bar{\ }), \tag{82}$$

where $\tau_{(m)}$ and $\tau_{(c)}$ are defined as follows:

$$\tau_{(\ )}(\mathbf{x},\omega) = \left[\left(\ _1(\omega)\frac{\nu(\omega)}{g^2}\right)^2 + \left(\ _2(\omega)\frac{|\bar{\ }|}{g}\right)^2\right]^{-1/2}, \tag{83}$$

$$\tau_{)}(\mathbf{x},\omega) = \left[\nu(\omega)^2 + \left(\frac{\ _2(\omega)\,|\bar{\ }|\,g}{\ _1(\omega)}\right)^2\right]^{1/2}, \tag{84}$$

where $c_1(\omega)$ and $c_2(\omega)$ are in general random constants and h is a mesh parameter. The uncertainty in Eqs. (83) and (84) comes from the randomness in large scale velocity $\bar{\ }$, the random kinematic viscosity $\nu(\omega)$ and the random constants $c_1(\omega)$ and $c_2(\omega)$. Again, caution needs to be exerted when using probability models with unbounded support space for modeling input uncertainty. In particular, all numerical studies were conducted in this report with $c_1 = 4$ and $c_2 = 2$. Furthermore the following relations hold via integration by parts:

$$(\bar{\ }\cdot\nabla\ ',\bar{\ }) = -(\ ',\bar{\ }\cdot\nabla\bar{\ }), \tag{85}$$

$$(\nu\nabla\ ',\nabla\bar{\ })_{\mathrm{v}} = -(\ ',\nu\Delta\bar{\ }). \tag{86}$$

Note that the second relation requires a twice differentiable velocity field and thus is an imposed strong regularity condition. Using the above relations and the subgrid scale models for velocity and pressure, we can simplify the large scale Eqs. (70) and (71) as follows:

$$\begin{aligned}&(\partial \bar{\ }, \bar{\ } + \tau_{(\ )}\{\bar{\ }\cdot\nabla\bar{\ } + \nu\Delta\bar{\ }\}) + (\nabla\bar{\ }, \tau_{(\ )}\{\bar{\ }\cdot\nabla\bar{\ } + \nu\Delta\bar{\ }\}) + (\bar{\ }\cdot\nabla\bar{\ }, \bar{\ } + \tau_{(\ )}\{\bar{\ }\cdot\nabla\bar{\ } + \nu\Delta\bar{\ }\})\\ &\quad + (\nu\nabla\bar{\ }, \nabla\bar{\ })_{\mathrm{v}} - (\bar{\ }, \nabla\cdot\bar{\ }) + (\nabla\cdot\bar{\ }, \tau_{(\ )}\nabla\cdot\bar{\ }) - (\nu\Delta\bar{\ }, \tau_{(\ )}\{\bar{\ }\cdot\nabla\bar{\ } + \nu\Delta\bar{\ }\})\\ &= (\cdot\ , \bar{\ } + \tau_{(\ )}\{\bar{\ }\cdot\nabla\bar{\ } + \nu\Delta\bar{\ }\}),\end{aligned} \tag{87}$$

$$(\nabla\cdot\bar{\ }, \bar{\ }) + (\partial\bar{\ }, \tau_{(\ )}\nabla\bar{\ }) + (\bar{\ }\cdot\nabla\bar{\ }, \tau_{(\ )}\nabla\bar{\ }) - (\nu\Delta\bar{\ }, \tau_{(\ )}\nabla\bar{\ }) + (\nabla\bar{\ }, \tau_{(\ )}\nabla\bar{\ }) = (\cdot\ , \tau_{(\ )}\nabla\bar{\ }). \tag{88}$$

5. Finite element implementation

5.1. Implementation of the stochastic advection–diffusion problem

Consider the set of elements resulting from the finite element discretization of the computational domain $\mathscr{D}$ as the set $\mathscr{E} = \{\mathscr{D}^{(F)}\}, F = 1, \ldots, \mathrm{Nel}$. We associate the large scale function spaces for the solution with finite element interpolation spaces $\mathscr{U}^{\bar{s}}$ and the trial function space with the space of stochastic Galerkin weighting functions $\mathscr{V}^{\bar{s}}$. Since the trial functions have to be stochastic we consider a new finite element basis formed as a tensor product of Galerkin shape functions over space and the generalized polynomial chaos basis for discretization over the probability space. This new basis is addressed as the stochastic Galerkin basis. Thus a weighting function $\bar{s} \in \mathscr{V}^{\bar{s}}$ has the functional form

$$\bar{s}(\mathbf{x}, \omega) = N(\mathbf{x})\psi(\omega), \tag{89}$$

where $N(\mathbf{x})$ denotes the deterministic finite element shape function and $\psi(\omega)$ denotes a member of the generalized polynomial chaos basis. Further, considering only linear finite elements for spatial discretization, the variational form given in Eq. (37) can be simplified as

$$\begin{aligned}&\int_{\mathscr{D}}\int_{\Omega} \bar{\ }^{\bar{s}}\left(\frac{\partial\bar{\phi}^{\bar{s}}}{\partial} + \mathbf{a}\cdot\nabla\bar{\phi}^{\bar{s}}\right) \mathrm{d}\mathscr{P}\,\mathrm{d}\mathbf{x} + \int_{\mathscr{D}}\int_{\Omega} \nu(\omega)\nabla\bar{\phi}^{\bar{s}}\cdot\nabla\bar{\ }^{\bar{s}}\,\mathrm{d}\mathscr{P}\,\mathrm{d}\mathbf{x}\\ &\quad + \mathop{\mathrm{A}}_{F=1}^{\mathrm{Nel}} \int_{\mathscr{D}^{(F)}}\int_{\Omega}\left(\frac{\partial\bar{\phi}^{\bar{s}}}{\partial} + \mathbf{a}\cdot\nabla\bar{\phi}^{\bar{s}}\right)\tau(\mathbf{x}, \omega)\mathbf{a}\cdot\nabla\bar{\ }^{\bar{s}}\,\mathrm{d}\mathscr{P}\,\mathrm{d}\mathbf{x}\\ &= \int_{\mathscr{D}}\int_{\Omega} \bar{\ }^{\bar{s}}\cdot\,\mathrm{d}\mathscr{P}\,\mathrm{d}\mathbf{x} + \mathop{\mathrm{A}}_{F=1}^{\mathrm{Nel}} \int_{\mathscr{D}^{(F)}}\int_{\Omega} \tau(\mathbf{x}, \omega)\mathbf{a}\cdot\nabla\bar{\ }^{\bar{s}}\cdot\,\mathrm{d}\mathscr{P}\,\mathrm{d}\mathbf{x}.\end{aligned} \tag{90}$$

The solution $\bar{\phi}^{\bar{s}}$ can be expressed in terms of a truncated generalized polynomial chaos expansion GPCE as

$$\bar{\phi}^{\bar{s}}(\mathbf{x},\ ,\omega) = \sum_{\ =0}^{P} \bar{\phi}^{\bar{s}}_{\ }(\mathbf{x},\ )\psi_{\ }(\omega), \tag{91}$$

where $\{\psi_{\ }(\omega)\}_0^P$ is the truncated generalized polyomial chaos basis. Further, the coefficients in above expansion lend themselves to a finite element representation in each element

$$\bar{\phi}^{\bar{s}}_{\ }(\mathbf{x},\ ) = \sum_{\beta=1}^{\mathrm{nbf}} \bar{\phi}_{\ \beta}(\ )N_{\beta}(\mathbf{x}), \tag{92}$$

where $N_\beta(\mathbf{x})$ are the standard Galerkin shape functions. This interpretation immediately helps identify the finite element interpolation of the following form:

$$\bar{\phi}^{s}(\mathbf{x},\ ,\omega)=\sum_{\ =0}^{P}\sum_{\beta=1}^{\mathrm{nbf}}\bar{\phi}^{s}_{\ ,\beta}(\ )N_\beta(\mathbf{x})\psi_{\ }(\omega). \tag{93}$$

This expression is also consistent with the tensor product finite element basis representation given in Eq. (89).

The spatial and probability space discretization of Eq. (90) yields the following set of ordinary differential equations

$$[\mathbf{M}+\mathbf{M}_\delta]\{\dot{\bar{\phi}}\}+[\mathbf{K}+\mathbf{N}+\mathbf{N}_\delta]\{\bar{\phi}\}=\{F\}, \tag{94}$$

where $\{\bar{\phi}\}$ if the vector of nodal values of $\bar{\phi}^{s}$. The nodal unknowns correspond to the terms in polynomial chaos expansion of $\bar{\phi}$. Further, $\{\dot{\bar{\phi}}\}$ denotes the time derivative of $\bar{\phi}$. The individual matrices are defined as follows with:

$$^{s}(\mathbf{x},\omega)=N_\alpha(\mathbf{x})\psi_{\ }(\omega),\qquad =(\alpha-1)(P+1)+\ , \tag{95}$$

$$_{\eta}^{s}(\mathbf{x},\omega)=N_\beta(\mathbf{x})\psi_{\ }(\omega),\quad _{\eta}=(\beta-1)(P+1)+\ , \tag{96}$$

$$[\mathbf{M}+\mathbf{M}_\delta]_{\ \eta}=\overset{\mathrm{Nel}}{\underset{e=1}{\mathsf{A}}}\int_{\mathscr{D}^{(e)}}\int_{\Omega}{}_{\eta}^{s}(\ ^{s}+\tau(\mathbf{x},\omega)\mathbf{a}\cdot\nabla\ ^{s})\,\mathrm{d}\mathscr{P}\,\mathrm{d}\mathbf{x}, \tag{97}$$

$$[\mathbf{K}+\mathbf{N}+\mathbf{N}_\delta]_{\ \eta}=\overset{\mathrm{Nel}}{\underset{e=1}{\mathsf{A}}}\int_{\mathscr{D}^{(e)}}\int_{\Omega}\left(\nu(\omega)\nabla\ {}_{\eta}^{s}\cdot\nabla\ ^{s}+\mathbf{a}\cdot\nabla\ {}_{\eta}^{s}(\ ^{s}+\tau(\mathbf{x},\omega)\mathbf{a}\cdot\nabla\ ^{s})\right)\mathrm{d}\mathscr{P}\,\mathrm{d}\mathbf{x}, \tag{98}$$

$$\{F\}\ =\overset{\mathrm{Nel}}{\underset{e=1}{\mathsf{A}}}\int_{\mathscr{D}^{(e)}}\int_{\Omega}{}_{\ }(\ ^{s}+\tau(\mathbf{x},\omega)\mathbf{a}\cdot\nabla\ ^{s})\,\mathrm{d}\mathscr{P}\,\mathrm{d}\mathbf{x}. \tag{99}$$

In the equations above, m and n denote the indices of a tensor-product finite element basis function (see Eqs. (95) and (96)), where $\alpha,\beta=1,\ldots,\mathrm{nbf}$, $r=0,\ldots,P$. Thus the indices m, n refer to the combination of the spatial and random bases given as $m,n=0,\ldots,(\mathrm{nbf}\times(P+1)-1)$.

The time integration is performed using the predictor–multicorrector algorithm that uses a one step generalized trapezoidal rule.

5.2. Implementation of the stochastic Navier–Stokes equations

Consider a finite element discretization similar to the stochastic advection–diffusion problem. The large scale velocity and pressure spaces are associated with the finite element spaces $\mathscr{W}^{s}$ and $\mathscr{X}^{s}$, respectively. The large scale trial function spaces are associated with the space of stochastic Galerkin functions $\mathscr{V}^{s}$ and $\mathscr{X}_0^{s}$. The variational form given in Eqs. (87) and (88) can be simplified for linear finite elements as follows:

$$\begin{aligned}
&\int_{\mathscr{D}}\int_{\Omega}\left(\frac{\partial^{-s}}{\partial}+{}^{-s}\cdot\nabla^{-s}\right)\cdot\ {}^{-s}\,\mathrm{d}\mathscr{P}\,\mathrm{d}\mathbf{x}+\int_{\mathscr{D}}\int_{\Omega}\nu(\omega)\nabla^{-s}:\nabla^{-s}\,\mathrm{d}\mathscr{P}\,\mathrm{d}\mathbf{x}\\
&\quad+\overset{\mathrm{Nel}}{\underset{e=1}{\mathsf{A}}}\int_{\mathscr{D}^{(e)}}\int_{\Omega}\left(\frac{\partial^{-s}}{\partial}+{}^{-s}\cdot\nabla^{-s}\right)\cdot\tau_{(\ )}{}^{-s}\cdot\nabla^{-s}\,\mathrm{d}\mathscr{P}\,\mathrm{d}\mathbf{x}-\int_{\mathscr{D}}\int_{\Omega}{}^{-s}\nabla\cdot\ {}^{-s}\,\mathrm{d}\mathscr{P}\,\mathrm{d}\mathbf{x}\\
&\quad+\overset{\mathrm{Nel}}{\underset{e=1}{\mathsf{A}}}\int_{\mathscr{D}^{(e)}}\int_{\Omega}\tau_{(\ )}\nabla^{-s}\cdot({}^{-s}\cdot\nabla^{-s})\,\mathrm{d}\mathscr{P}\,\mathrm{d}\mathbf{x}+\overset{\mathrm{Nel}}{\underset{e=1}{\mathsf{A}}}\int_{\mathscr{D}^{(e)}}\int_{\Omega}\tau_{(\ )}\nabla\cdot{}^{-s}\nabla\cdot{}^{-s}\,\mathrm{d}\mathscr{P}\,\mathrm{d}\mathbf{x}\\
&=\int_{\mathscr{D}}\int_{\Omega}{}_{\ }\cdot\ {}^{-s}\,\mathrm{d}\mathscr{P}\,\mathrm{d}\mathbf{x}+\overset{\mathrm{Nel}}{\underset{e=1}{\mathsf{A}}}\int_{\mathscr{D}^{(e)}}\int_{\Omega}\tau_{(\ )}{}_{\ }\cdot({}^{-s}\cdot\nabla^{-s})\,\mathrm{d}\mathscr{P}\,\mathrm{d}\mathbf{x},
\end{aligned} \tag{100}$$

$$\int_{\mathscr{D}}\int_{\Omega}\nabla\cdot{}^{-}{}^{s}{}^{-}{}^{s}\,\mathrm{d}\mathscr{P}\,\mathrm{d}\mathbf{x}+\overset{\mathrm{Nel}}{\underset{e=1}{\mathsf{A}}}\int_{\mathscr{D}_e^{(F)}}\int_{\Omega}\left(\frac{\partial^{-}{}^{s}}{\partial}+{}^{-}{}^{s}\cdot\nabla^{-}{}^{s}\right)\cdot(\tau_{(\ )}\nabla^{-}{}^{s})\,\mathrm{d}\mathscr{P}\,\mathrm{d}\mathbf{x}$$
$$+\overset{\mathrm{Nel}}{\underset{e=1}{\mathsf{A}}}\int_{\mathscr{D}_e^{(F)}}\int_{\Omega}\nabla^{-}{}^{s}\cdot(\tau_{(\ )}\nabla^{-}{}^{s})\,\mathrm{d}\mathscr{P}\,\mathrm{d}\mathbf{x}$$
$$=\overset{\mathrm{Nel}}{\underset{e=1}{\mathsf{A}}}\int_{\mathscr{D}_e^{(F)}}\int_{\Omega}\cdot(\tau_{(\ )}\nabla^{-}{}^{s})\,\mathrm{d}\mathscr{P}\,\mathrm{d}\mathbf{x}. \tag{101}$$

By considering similar finite element expression as in Eq. (93), we obtain after spatial discretization, the following nonlinear system of ordinary differential equations:

$$[\mathbf{M}+\mathbf{M}_{\delta}]\{\dot{}\}+[\mathbf{K}+\mathbf{N}(^{-})+\mathbf{N}_{\delta}(^{-})+\mathbf{C}]\{^{-}\}-[\mathbf{G}+\mathbf{G}_{\delta}]\{^{-}\}=\{F\}+\{F_{\delta}\}, \tag{102}$$

$$[\mathbf{G}^{\mathrm{T}}]\{^{-}\}+[\mathbf{M}_{\varepsilon}]\{\dot{}\}+[\mathbf{N}_{\varepsilon}(^{-})]\{^{-}\}+[\mathbf{G}_{\varepsilon}]\{^{-}\}=\{F_{\varepsilon}\}, \tag{103}$$

where the individual matrices are defined as follows:

$$[\mathbf{M}+\mathbf{M}_{\delta}]_{\mathbf{mn}}=\overset{\mathrm{Nel}}{\underset{e=1}{\mathsf{A}}}\int_{\mathscr{D}_e^{(F)}}\int_{\Omega}(\ {}^{s}+\tau_{(\ )}(\mathbf{x},\omega)^{-}{}^{s}\cdot\nabla\ {}^{s})\ {}^{s}_{\eta}\delta_{l}\,\mathrm{d}\mathscr{P}\,\mathrm{d}\mathbf{x}, \tag{104}$$

$$[\mathbf{K}]_{\mathbf{mn}}=\overset{\mathrm{Nel}}{\underset{e=1}{\mathsf{A}}}\int_{\mathscr{D}_e^{(F)}}\int_{\Omega}\left(v(\omega)\ {}^{s}_{,}\ {}^{s}_{\eta,}\delta_{l}+v(\omega)\ {}^{s}_{l}\ {}^{s}_{\eta,}\right)\mathrm{d}\mathscr{P}\,\mathrm{d}\mathbf{x}, \tag{105}$$

$$[\mathbf{N}+\mathbf{N}_{\delta}]_{\mathbf{mn}}=\overset{\mathrm{Nel}}{\underset{e=1}{\mathsf{A}}}\int_{\mathscr{D}_e^{(F)}}\int_{\Omega}(\ {}^{s}+\tau_{(\ )}(\mathbf{x},\omega)^{-}{}^{s}\cdot\nabla\ {}^{s})^{-}{}^{s}\cdot\nabla\ {}^{s}_{\eta}\delta_{l}\,\mathrm{d}\mathscr{P}\,\mathrm{d}\mathbf{x}, \tag{106}$$

$$[\mathbf{C}]_{\mathbf{mn}}=\overset{\mathrm{Nel}}{\underset{e=1}{\mathsf{A}}}\int_{\mathscr{D}_e^{(F)}}\int_{\Omega}\tau_{(\ )}(\mathbf{x},\omega)\nabla\cdot\ {}^{s}\nabla\cdot\ {}^{s}_{\eta}\,\mathrm{d}\mathscr{P}\,\mathrm{d}\mathbf{x}, \tag{107}$$

$$[\mathbf{G}+\mathbf{G}_{\delta}]_{\mathbf{mn}}=\overset{\mathrm{Nel}}{\underset{e=1}{\mathsf{A}}}\int_{\mathscr{D}_e^{(F)}}\int_{\Omega}\left(\ {}^{s}_{,}\ {}^{s}_{\eta}-\tau_{(\ )}(\mathbf{x},\omega)^{-}{}^{s}\cdot\nabla\ {}^{s}\ {}^{s}_{\eta,}\right)\mathrm{d}\mathscr{P}\,\mathrm{d}\mathbf{x}, \tag{108}$$

$$\{F+F_{\delta}\}_{\mathbf{m}}=\overset{\mathrm{Nel}}{\underset{e=1}{\mathsf{A}}}\int_{\mathscr{D}_e^{(F)}}\int_{\Omega}(\ {}^{s}+\tau_{(\ )}(\mathbf{x},\omega)^{-}{}^{s}\cdot\nabla\ {}^{s})_{\cdot}\,\mathrm{d}\mathscr{P}\,\mathrm{d}\mathbf{x}, \tag{109}$$

$$[\mathbf{G}^{\mathrm{T}}]_{\mathbf{mn}}=\overset{\mathrm{Nel}}{\underset{e=1}{\mathsf{A}}}\int_{\mathscr{D}_e^{(F)}}\int_{\Omega}\ {}^{s}\ {}^{s}_{\eta\,l}\,\mathrm{d}\mathscr{P}\,\mathrm{d}\mathbf{x}, \tag{110}$$

$$[\mathbf{M}_{\varepsilon}]_{\mathbf{mn}}=\overset{\mathrm{Nel}}{\underset{e=1}{\mathsf{A}}}\int_{\mathscr{D}_e^{(F)}}\int_{\Omega}\ {}^{s}_{\eta}\tau_{(\ )}(\mathbf{x},\omega)\ {}^{s}_{l}\,\mathrm{d}\mathscr{P}\,\mathrm{d}\mathbf{x}, \tag{111}$$

$$[\mathbf{N}_{\varepsilon}]_{\mathbf{mn}}=\overset{\mathrm{Nel}}{\underset{e=1}{\mathsf{A}}}\int_{\mathscr{D}_e^{(F)}}\int_{\Omega}{}^{-}{}^{s}\cdot\nabla\ {}^{s}_{\eta}\tau_{(\ )}(\mathbf{x},\omega)\ {}^{s}_{l}\,\mathrm{d}\mathscr{P}\,\mathrm{d}\mathbf{x}, \tag{112}$$

$$[\mathbf{G}_{\varepsilon}]_{\mathbf{mn}}=\overset{\mathrm{Nel}}{\underset{e=1}{\mathsf{A}}}\int_{\mathscr{D}_e^{(F)}}\int_{\Omega}\tau_{(\ )}(\mathbf{x},\omega)\ {}^{s}_{,}\ {}^{s}_{\eta,}\,\mathrm{d}\mathscr{P}\,\mathrm{d}\mathbf{x}, \tag{113}$$

$$\{F_{\varepsilon}\}_{\mathbf{m}}=\overset{\mathrm{Nel}}{\underset{e=1}{\mathsf{A}}}\int_{\mathscr{D}_e^{(F)}}\int_{\Omega}\tau_{(\ )}(\mathbf{x},\omega)\ {}^{s}_{l}\cdot\,\mathrm{d}\mathscr{P}\,\mathrm{d}\mathbf{x}. \tag{114}$$

The time integration is performed using the predictor–multicorrector algorithm that uses a one step generalized trapezoidal rule.

Remark 3. As of now, no explicit numerical convergence theorems have been proved for stochastic PDEs with the variational multiscale method. However, we conjecture that since the proposed subgrid models yield a stabilization FE scheme similar to Galerkin least squares GLS [44], the convergence in spatial sense will be similar to that of the GLS method. The convergence in stochastic sense is governed by the Cameron and Martin theorem [9] for stochastic processes represented in an infinite generalized polynomial chaos expansion. However, further detailed investigation is required for truncated generalized polynomial chaos representations. The authors feel that the combination of GLS convergence analysis and the Cameron–Martin theorem can yield convergence results for the proposed approach. Further research is needed in this regard.

5.2.1. Solution of the linear system of equations

In this work, we use the parallel preconditioned GMRES algorithm proposed by Tezduyar et al. [45–47] for the solution of linear equations resulting from the finite element discretization. The parameters needed by the algorithm include the dimension of the Krylov basis, the tolerance for termination of the Arnoldi iterations, the number of GMRES outer iteration restarts and the type of the preconditioner.

The parallel GMRES solver used in this work employs two different preconditioners, in particular, a basis diagonal preconditioner and a more complicated Crouts preconditioner that uses incomplete LU factorization. It was found by numerical experiments that for all problems in this work, a Krylov basis of dimension 30 and number of restarts equal to 15 resulted in convergence to a value less than $1e-09$. Except for the flow past a circular cylinder problem all other examples used the diagonal preconditioner.

The matrix–vector operations and the vector–vector operations were performed using an efficient cluster dependent implementation of BLAS I and BLAS II. Further discussion of the programming logic is beyond the breadth of this report and hence is not resorted to.

6. Numerical examples

In the subsequent numerical examples, we consider uncertainty in boundary conditions and advection velocity for stochastic advection–diffusion problems and uncertainty in inlet velocity for stochastic incompressible fluid-flow problems. For all the uncertain input, an uniform probability distribution model is used, since the uniform model represents the most basic non-informative prior model for an uncertain input (typically used when someone knows only the maximum and minimum values).

6.1. Steady advection skew to a mesh

The problem statement is depicted in Fig. 1. The flow is taken to be unidirectional, skew to the mesh. The advection velocity is modeled as a two-dimensional random variable. The randomness in velocity translates as the randomness in the angle of skew $\alpha = \tan^{-1}(a_2/a_1)$, where a_1 and a_2 are the x and y components of the velocity, respectively. The inflow boundary conditions are discontinuous as shown in Fig. 1. Homogenous natural boundary conditions are applied to the outflow boundary.

In the presence of negligible diffusion, the stochastic solution to this problem is essentially a pure advection of the discontinuous inflow boundary condition along flow characteristics. In particular, the solution can be written in terms of the characteristic emanating from the point $(-0.5,-0.25)$ as follows:

$$\phi(\mathbf{x},\omega) = \phi_f(\omega)\mathbb{I}_{[\mathbf{x},\omega;\mathbf{g}(\mathbf{x},\omega)\leqslant 0]}(\mathbf{x},\omega), \tag{115}$$

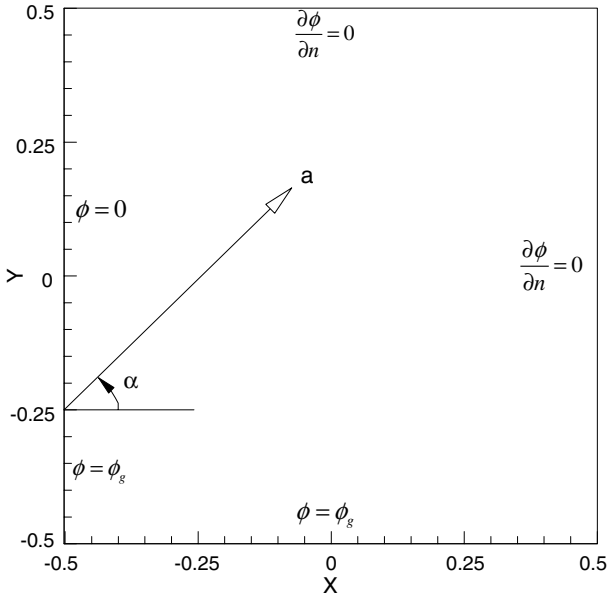

Fig. 1. Schematic of problem definition for steady advection skew to a mesh.

where the function $h(\mathbf{x},\omega)$ is defined as follows:

$$\mathcal{S}(\mathbf{x},\omega) = \left(+ \tfrac{1}{4} \right)\ {}_1(\omega) - \left(+ \tfrac{1}{2} \right)\ {}_2(\omega) \tag{116}$$

and $I_{[A]}$ is the indicator function for the set A

$$\mathbb{I}_{[A]}(\mathbf{x}) = \begin{cases} 1, & \mathbf{x} \in A, \\ 0, & \text{otherwise.} \end{cases} \tag{117}$$

From Eq. (115) it is clear that the uncertainty in inflow boundary conditions and advection velocity affect the uncertainty in solution.

Remark 4. In deterministic SUPG algorithms, the solution exhibits stability and good numerical accuracy when the solution is regular. However, for non-regular solutions (e.g. solutions with discontinuities) the SUPG estimates are not valid in the neighborhood of the discontinuity. Typically spurious oscillations are observed in such locations. The proposed stabilized algorithm is a logical extension of SUPG-like methods for the solution of stochastic advection–diffusion equation. Hence, the behavior of the algorithm in the presence of discontinuities in solution is expected to mimic the behavior of SUPG like methods in deterministic case. The significance of this argument will be clear after viewing the cases below.

6.1.1. Case 1: No uncertainty in advection velocity, ϕ_g modeled as an uniform random variable

The advection velocity is taken to be a constant $\mathbf{a} = (1,1)^{\mathrm{T}}$. This results in a 45° angle of skew. The stochastic inflow boundary condition ϕ_g can be written as $\phi_g = 1 + \delta\xi$, where δ is a positive real number less than one and ξ is a random variable uniformly distributed between -1 and 1.

In this case, the exact stochastic solution can be written as

$$\phi(\mathbf{x},\omega) = (1 + \delta\xi)\mathbb{I}_{[\mathbf{x};\mathcal{S}(\mathbf{x}) \leqslant 0]}(\mathbf{x}), \tag{118}$$

where $h(\mathbf{x})$ is simplified as

$$g(\mathbf{x}) = \quad - \; - \tfrac{1}{4}. \tag{119}$$

The solution obtained with a second order Legendre chaos expansion for the solution is shown in Fig. 2. The model constant δ was taken to be 0.1. Except in the regions in the neighborhood of the solution discontinuity, the numerical solution is exact (refer to Remark 2). As predicted by Eq. (118), all higher order Legendre chaos coefficients in the expansion of $\phi(\mathbf{x},\omega)$ (excluding the mean and the first order term) were identically zero and hence are not plotted.

6.1.2. Case 2: No uncertainty in inflow boundary conditions, advection velocity modeled as a two-dimensional uniform random variable

The inflow boundary condition is taken to be constant $\phi_g = 1$. The advection velocity is modeled as a two-dimensional uniform random variable $\mathbf{a} = (1 + \delta\xi_1,\ 1 + \delta\xi_2)$, where δ is a positive real number, ξ_1 and ξ_2 are independent identically distributed (i.i.d) random variables uniformly distributed between -1 and 1.

We consider two subcases here, in the first case the diffusion coefficient is taken to be 0.001. The exact stochastic solution does not exist here. In the second case, we take the diffusion coefficient to be negligible. The exact solution to the second case can be written as

$$\phi(\mathbf{x},\omega) = \mathbb{I}_{[\mathbf{x},\omega;g(\mathbf{x},\omega)\leqslant 0]}(\mathbf{x},\omega), \tag{120}$$

where $h(\mathbf{x},\omega)$ is

$$g(\mathbf{x},\omega) = \left(\quad + \tfrac{1}{4}\right)(1+\delta\xi_1) - \left(- \tfrac{1}{2}\right)(1+\delta\xi_2). \tag{121}$$

At a given spatial location, Eq. (120) implies that $\phi(\mathbf{x},\omega)$ is distributed as a Bernoulli random variable. Thus, though the input uncertainty has a continuous distribution (uniformly distributed advection

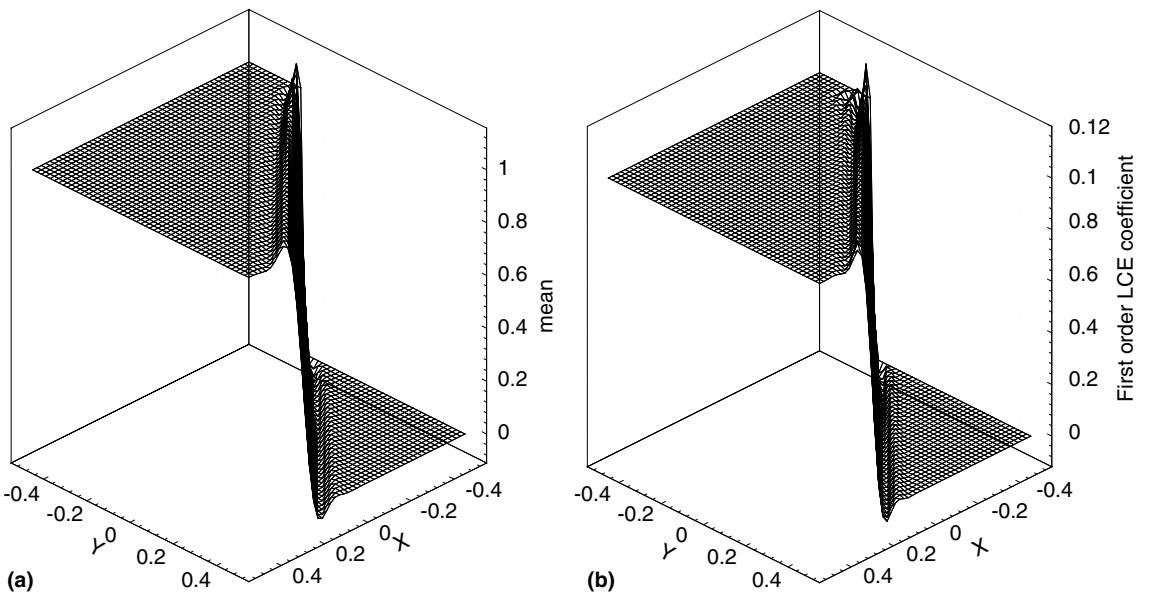

Fig. 2. Advection skew to a mesh, case 1: whole domain solution for a second-order Legendre chaos expansion of the solution (a) mean and (b) first-order term.

velocity), the output has a discrete probability distribution. Since in this stochastic version we have to capture distributions in both spatial solution and the probability distribution, the stochastic version is tougher to solve than the corresponding deterministic advection skew to a mesh problem.

Subcase 1 – diffusion coefficient k = 0.001: Computational investigations were performed for various mesh discretizations and orders of Legendre chaos approximation of the solution. Convergence was obtained for fourth-order Legendre chaos approximation. The criterion for convergence used in the example is as follows:

$$\varepsilon = \frac{\|\phi^{(\ +1)} - \phi^{(\ )}\|}{\|\phi^{(\ )}\|}, \tag{122}$$

where, the $\|\cdot\|$ is the $L_2(\Omega) \times L_2(\mathscr{D})$ norm, $\phi^{(p)}$ and $\phi^{(p\ +\ 1)}$ are the solutions from successive orders of Legendre chaos expansion of the solution. The converged error norm stabilized around 0.03 indicating a three percent error.

The solutions at various y-values and the whole domain mean and standard deviation obtained using a 50×50 mesh are shown in Fig. 3. The value of δ was taken to be 0.1. Excellent agreement is seen between the Monte-Carlo solution obtained after 100,000 iterations and the order 4 polynomial chaos solution. The whole domain solutions obtained for mean and standard deviation are shown in Fig. 4. Thus, for cases with appreciable diffusion, the proposed technique performs well. We shall now proceed to test the algorithm in the limit of pure advection. It is expected that the spurious oscillations in the vicinity of the sharp gradient layer will pollute the mean solution leading to unwanted errors in the estimation of higher order statistics. This however is a characteristic of all SUPG-like methods and has nothing to do with the order of Legendre chaos approximation used.

Subcase 2 – diffusion coefficient k = 0: Computational investigations were performed for various mesh discretizations and orders of Legendre chaos approximation of the solution. Convergence was obtained for a fourth-order Legendre chaos approximation. The criteria for convergence used in the example is as follows:

$$\varepsilon = \frac{\|\phi^{(\ )} - \phi^{\text{exact}}\|}{\|\phi^{\text{exact}}\|}, \tag{123}$$

where the $\|\cdot\|$ is the $L_2(\Omega) \times L_2(\mathscr{D})$ norm, $\phi^{(p)}$ is the solution from a pth-order Legendre chaos approximation of the solution. ϕ^{exact} is the exact solution. In this example, it was noticed that the error did not decay below 23%. This is attributed to the spurious behavior of the algorithm in the vicinity of sharp solution gradients. Further sophisticated subgrid modeling and introduction of discontinuous interpolation functions in the finite element method may be required to avoid these problems. However, it defeats the purpose of this work in establishing that simple models can be used to obtain fairly accurate results in many important advection–diffusion and flow problems. The solutions at various y-values and the whole domain mean and standard deviation obtained using a 50×50 mesh are shown in Fig. 5. The value of δ was taken to be 0.1. It can be observed that though the mean estimates are fairly accurate, the oscillations in the vicinity of the sharp layers in solution pollute the standard deviation. The whole domain solution for mean and standard deviation as obtained for a fourth-order Legendre chaos expansion of the output is given in Fig. 6.

6.2. Transient advection of a cosine hill in rotating flow field

The transient advection of a cosine hill in a rotating flow field has been identified as a standard test problem for testing advection–diffusion algorithms [48]. The problem definition is depicted in Fig. 7. The flow field comprises of rigid rotation about the origin (taken here to be the point (0,0)). Uncertainty here is

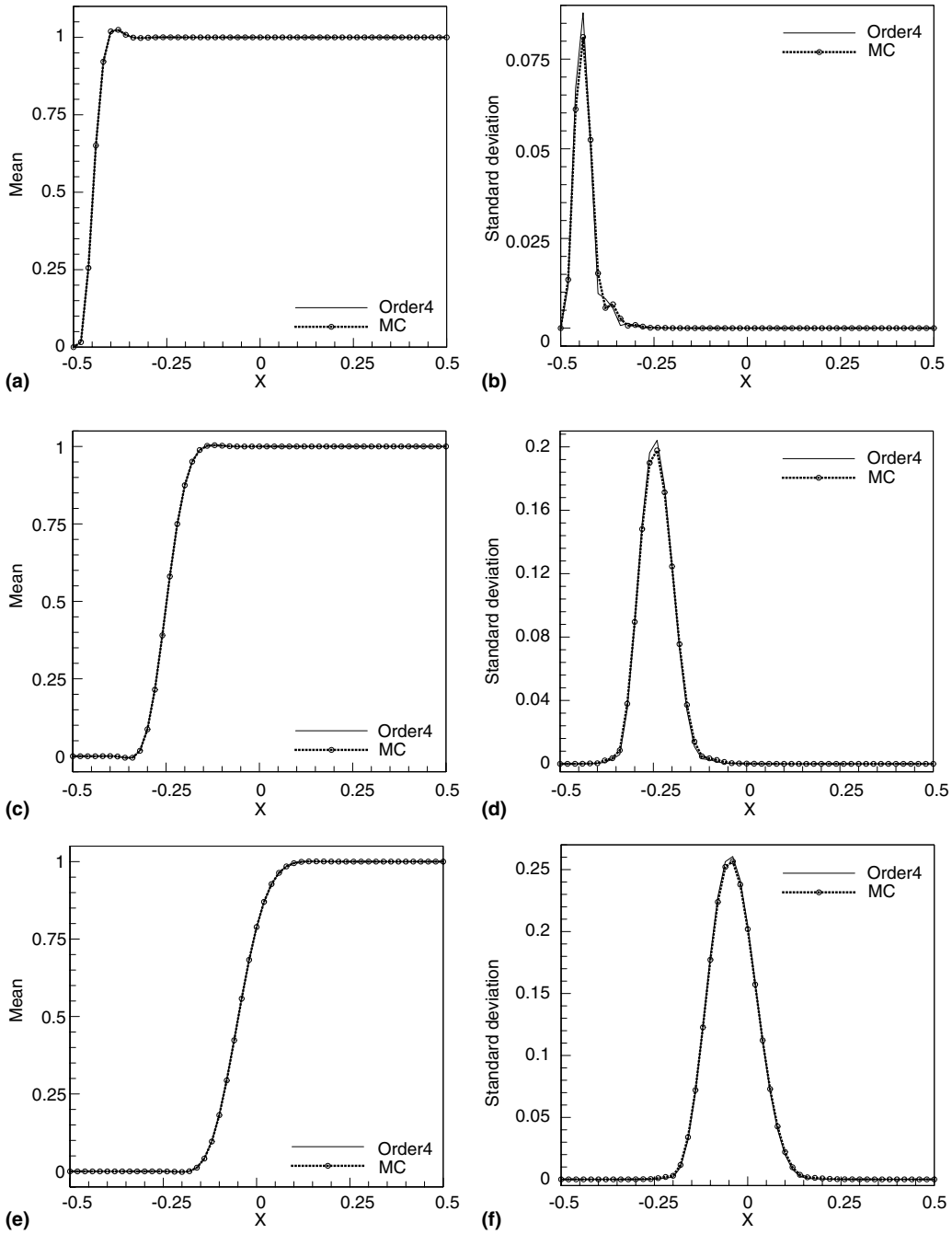

Fig. 3. Advection skew to a mesh, case 1 with $k = 0.001$: comparison between solution mean and standard deviation of solution obtained by 100,000 Monte-Carlo iterations and a fourth-order Legendre chaos solution approximation at various y values: (a) mean at $y = -0.2$; (b) standard deviation at $y = -0.2$; (c) mean at $y = 0$; (d) standard deviation at $y = 0$; (e) mean at $y = 0.2$; (f) standard deviation at $y = 0.2$.

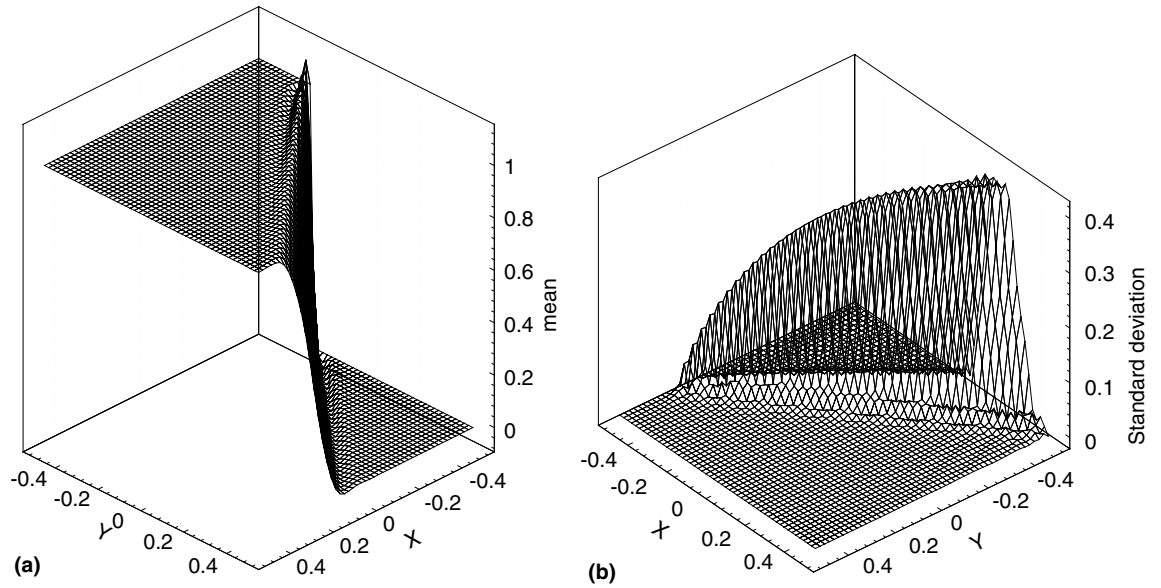

Fig. 4. Advection skew to a mesh, case 1 with $k = 0.001$: whole domain solutions for the (a) mean and (b) the standard deviation obtained for a fourth-order Legendre chaos approximation of the solution.

considered in the speed of rotation $\gamma(\omega)$. Initial conditions, boundary conditions are considered to be deterministic. We test the problem in the limit of pure advection (diffusion coefficient $\approx 10^{-9}$). The advection velocity hence has circular characteristics centered at the origin (0,0). Further, the advection velocity at any spatial location is given by

$$\mathbf{a}(\mathbf{x}, \ , \omega) = (\ _1(\mathbf{x}, \omega), \ _2(\mathbf{x}, \omega)) = (\gamma(\omega) \ , -\gamma(\omega)_{\gamma_{\psi}}). \tag{124}$$

The initial conditions for the problem were taken as follows:

$$\phi(\mathbf{x}, 0, \ ) = \mathbb{I}_{[\ : \ -0.2<0]}(\ ) \cos(5\pi \ /2), \tag{125}$$

where r is defined as

$$= \left[\left(_{\psi} - \tfrac{1}{4} \right)^2 + \ ^2 \right]^{1/2}. \tag{126}$$

In the limit of pure advection, the initial conditions propagate along the circular streamlines. The transient solution can hence be written as follows:

$$\phi(\mathbf{x}, \ , \omega) = \mathbb{I}_{[\hat{\ }:\hat{\ }-0.2<0]}(\hat{\ }) \cos(5\pi\hat{\ }/2), \tag{127}$$

where $\hat{\ }$ is defined as

$$\hat{\ } = ((_{\psi} - \hat{}_{\psi})^2 + (\ - \hat{\ })^2)^{1/2}, \quad \hat{}_{\psi} = \tfrac{1}{4}\cos(\gamma \ ), \quad \hat{\ } = \tfrac{1}{4}\sin(\gamma \ ). \tag{128}$$

The principal investigations in this example include: (i) a comparison of the mean stochastic solution $\mu_{\phi}(\mathbf{x})$ with the analytical mean; (ii) a comparison of the standard deviation of the stochastic solution $\sigma_{\phi}(\mathbf{x})$ with the analytical standard deviation; (iii) a discussion of numerical diffusion and phase lag.

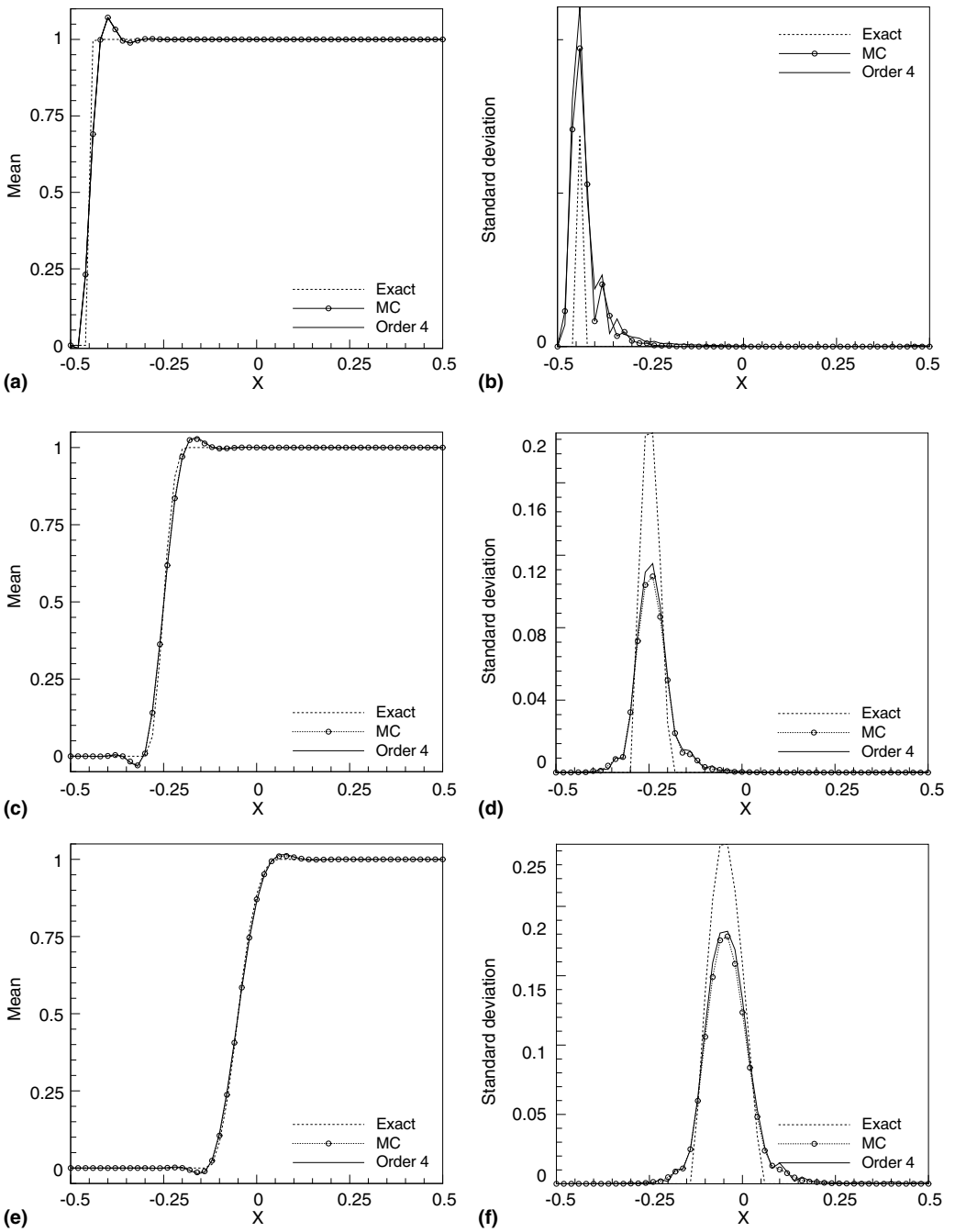

Fig. 5. Advection skew to a mesh, case 1 with $k = 0$: comparison between solution mean and standard deviation of solution obtained by 100,000 Monte-Carlo iterations and a fourth-order Legendre chaos solution approximation at various y values: (a) mean at $y = -0.2$; (b) standard deviation at $y = -0.2$; (c) mean at $y = 0$; (d) standard deviation at $y = 0$; (e) mean at $y = 0.2$; (f) standard deviation at $y = 0.2$.

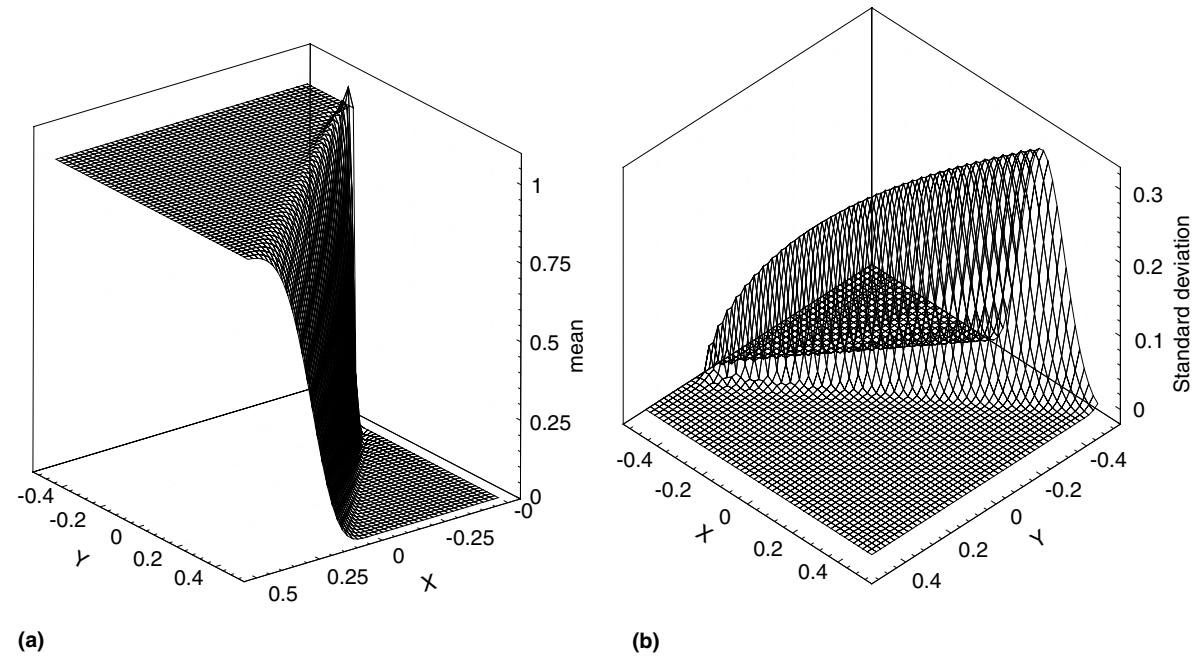

Fig. 6. Advection skew to a mesh, case 1 with $k = 0.001$: whole domain solutions for the (a) mean and (b) the standard deviation obtained for a fourth-order Legendre chaos approximation of the solution.

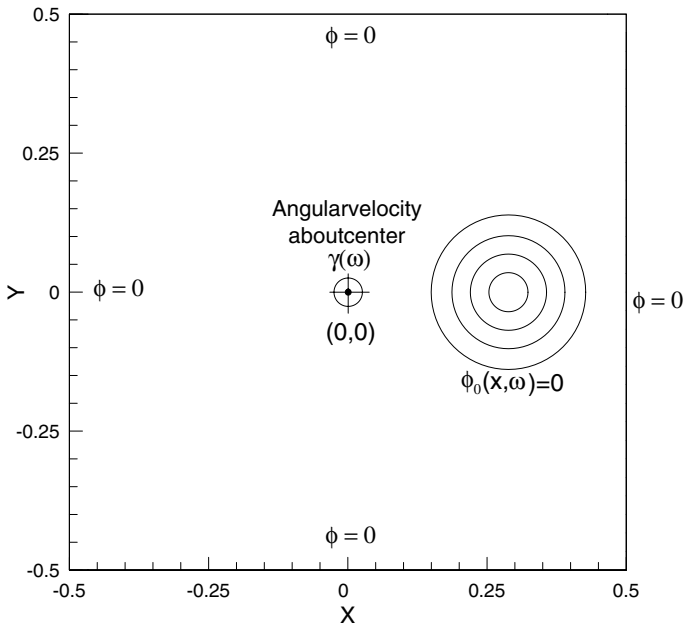

Fig. 7. Problem definition for transient advection of a cosine hill in a rotating flow field.

6.2.1. Computational details

A 50×50 mesh of uniform bilinear isoparametric quadrilateral elements is used for computation. The speed of rotation γ is modeled as a uniform random variable

$$\gamma(\omega) = 1 + \delta\xi(\omega), \quad \xi \overset{\mathrm{d}}{=} \mathrm{unif}(-1, 1), \tag{129}$$

where δ is a positive real constant less than one.

The simulation was carried up to non-dimensional time $t = 9$ with a time stepping of $\Delta t = 0.0025$. The predictor–multicorrector algorithm was used for time integration. The model constant δ was taken to be 0.1. This value corresponds to a 10% fluctuation in speed of rotation about the mean value.

Since the exact stochastic solution given by Eq. (127) is not amenable to further simplifications, it is computed using 100,000 Monte-Carlo realizations (convergence was obtained around 60,000 iterations).

The phase errors, visible as spurious leading and lagging oscillations in solution are absent for all orders of Legendre chaos approximation of the solution. The converged solution was obtained for a fourth-order Legendre chaos approximation. The convergence criterion used here can be written as

$$\varepsilon = \frac{\|\phi^{(\ )} - \phi^{\mathrm{exact}}\|}{\|\phi^{\mathrm{exact}}\|}, \tag{130}$$

where, the $\|\cdot\|$ is the $L_2(\Omega) \times L_2(\mathscr{D})$ norm, $\phi^{(p)}$ is the solution from a pth-order Legendre chaos approximation of the solution. ϕ^{exact} is the exact solution as computed by MC iterations.

The peak error in a quantity q is defined as

$$\varepsilon = \frac{\max \quad - \max \ _{\mathrm{exact}}}{\max \ _{\mathrm{exact}}}. \tag{131}$$

The contour plots comparing the mean and standard deviation with the exact solution (obtained by 100,000 MC iterations) are shown in Fig. 8(a)–(f). It can be observed that though the mean solution is almost exact for a second-order approximation, the standard deviation contours bear no resemblance to the exact solution. However, for a fourth-order approximation, the mean and standard deviation show excellent agreement with the exact solution. Further, the peak error in the mean and standard deviation are found to be around 3.5% and 5%, respectively. This numerical diffusion is a characteristic of any SUPG like method and is well within the limits of numerical diffusion seen in deterministic problems.

The whole domain converged solution corresponding to fourth-order solution approximation is given in Fig. 9.

6.3. Internal channel flow: Poiselle flow

This example is chosen for its simplicity and existence of an analytical stochastic solution for the velocity field. It was examined earlier in [10] using a spectral projection method with the fractional step implementation of the Navier–Stokes equations. The solution is two-dimensional in the initial transition zone. Then the solution is completely one-dimensional in the so-called fully-developed region.

The schematic with the problem definition and mesh details used here are given in Fig. 10. The computational mesh is comprised of 100×10 bilinear quadrilateral elements. The inlet velocity is axial with a magnitude U that is uncertain. The inlet velocity U is modeled as a random variable with a uniform distribution $U[0.9,1.1]$. The kinematic viscosity is considered to be deterministic and is given the value 0.025. The Poiselle flow problem is addressed here as a transient problem. The simulation was carried out until steady-state was achieved at around $t \approx 22.5$ s with a time stepping of $\Delta t = 0.002$.

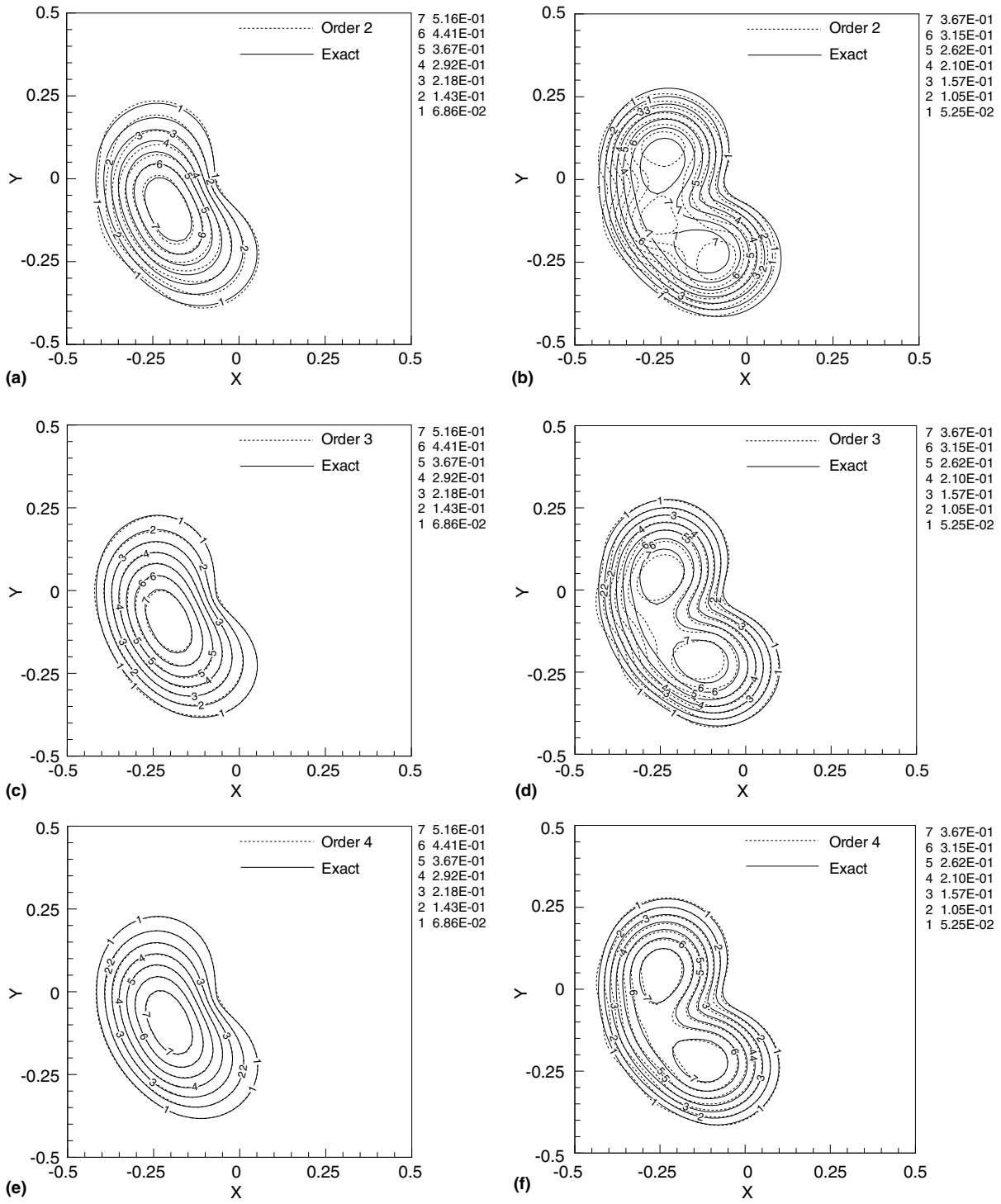

Fig. 8. Pure advection of a cosine hill in a rotating flow field: comparison of mean and standard deviation for various orders of Legendre chaos approximation of solution versus the exact solution (computed with 100,000 MC realizations).

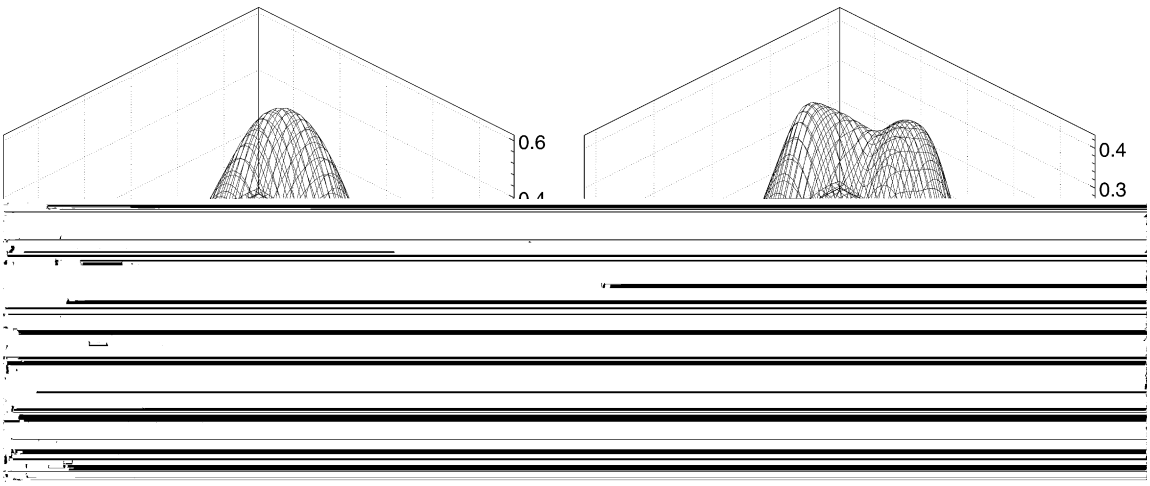

Fig. 9. Pure advection of a cosine hill in a rotating flow field: whole domain solutions for the (a) mean and (b) the standard deviation obtained for a fourth-order Legendre chaos approximation of the solution.

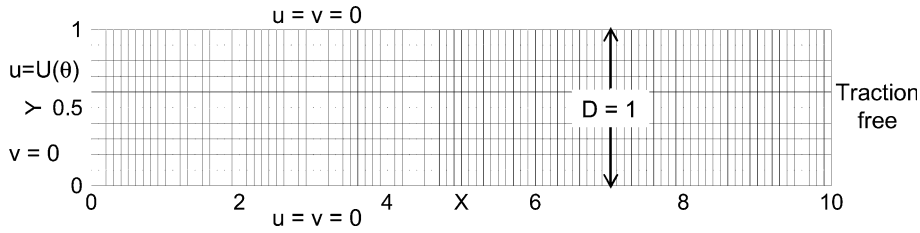

Fig. 10. Schematic of the computational domain and mesh details for the Poiselle flow example.

The flow Reynolds number is defined based on the channel width D as follows:

$$\mathrm{Re}(\omega) = \frac{(\omega)D}{v}. \tag{132}$$

No uncertainty is considered in the initial or boundary conditions. The analytical solution for the velocity in the fully-developed region at steady-state can be written as

$$\text{f}(\mathbf{x},\ ,\omega) = 4\ \ _D(\omega)\left(\frac{}{D}\right)\left[1-\left(\frac{}{D}\right)\right], \qquad (\mathbf{x},\ ,\omega) = 0, \tag{133}$$

where the maximum velocity at the center of the channel is given as $U_D = 1.5U(\omega)$.

The solution $u(\mathbf{x},t,\omega)$ can be further simplified as follows:

$$\text{f}(\mathbf{x},\ ,\omega) = \text{f}_0 + \text{f}_1\xi(\omega) = 4(1+0.1\xi(\omega))\ \ _D(\omega)\left(\frac{}{D}\right)\left[1-\left(\frac{}{D}\right)\right]. \tag{134}$$

The results for the mean axial velocity and its first coefficient in the Legendre-chaos expansion are shown in Fig. 11(a) and (b). It can be seen that the mean velocity results are nearly exact.

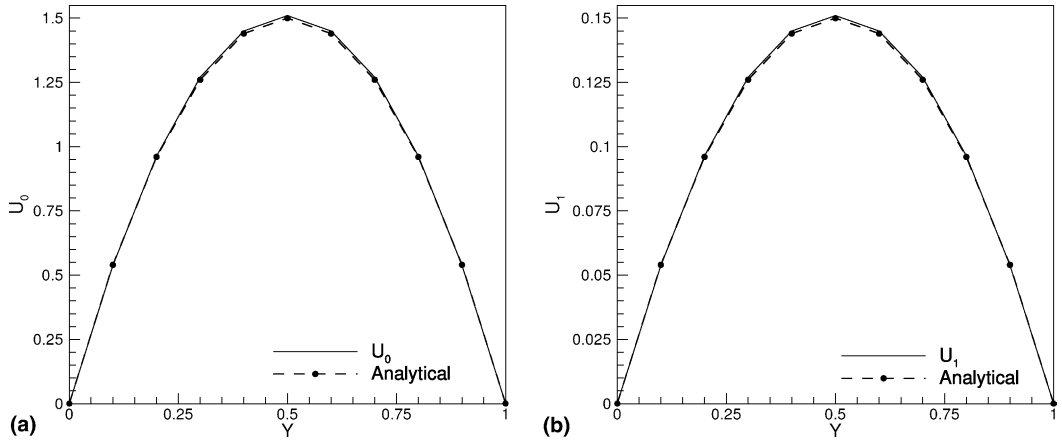

Fig. 11. Poiselle flow: (a) mean axial velocity; (b) first term in LCE of axial velocity.

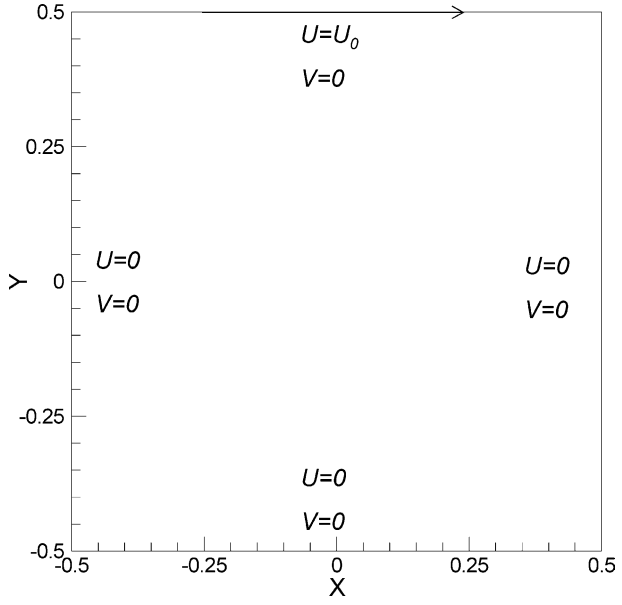

Fig. 12. Problem definition for the lid driven cavity example.

6.4. Driven cavity flows – lid driven square cavity problem

Over the last two decades, much interest has been given to the investigation of the classical driven cavity problem. Here, we consider the motion of an incompressible fluid within an impermeable square box. The fluid motion is driven by the uniform motion of one of the sides of the box (lid here). This problem has often provided a stiff test for fluid-flow solvers [49–52]. The presence of interesting phenomena like

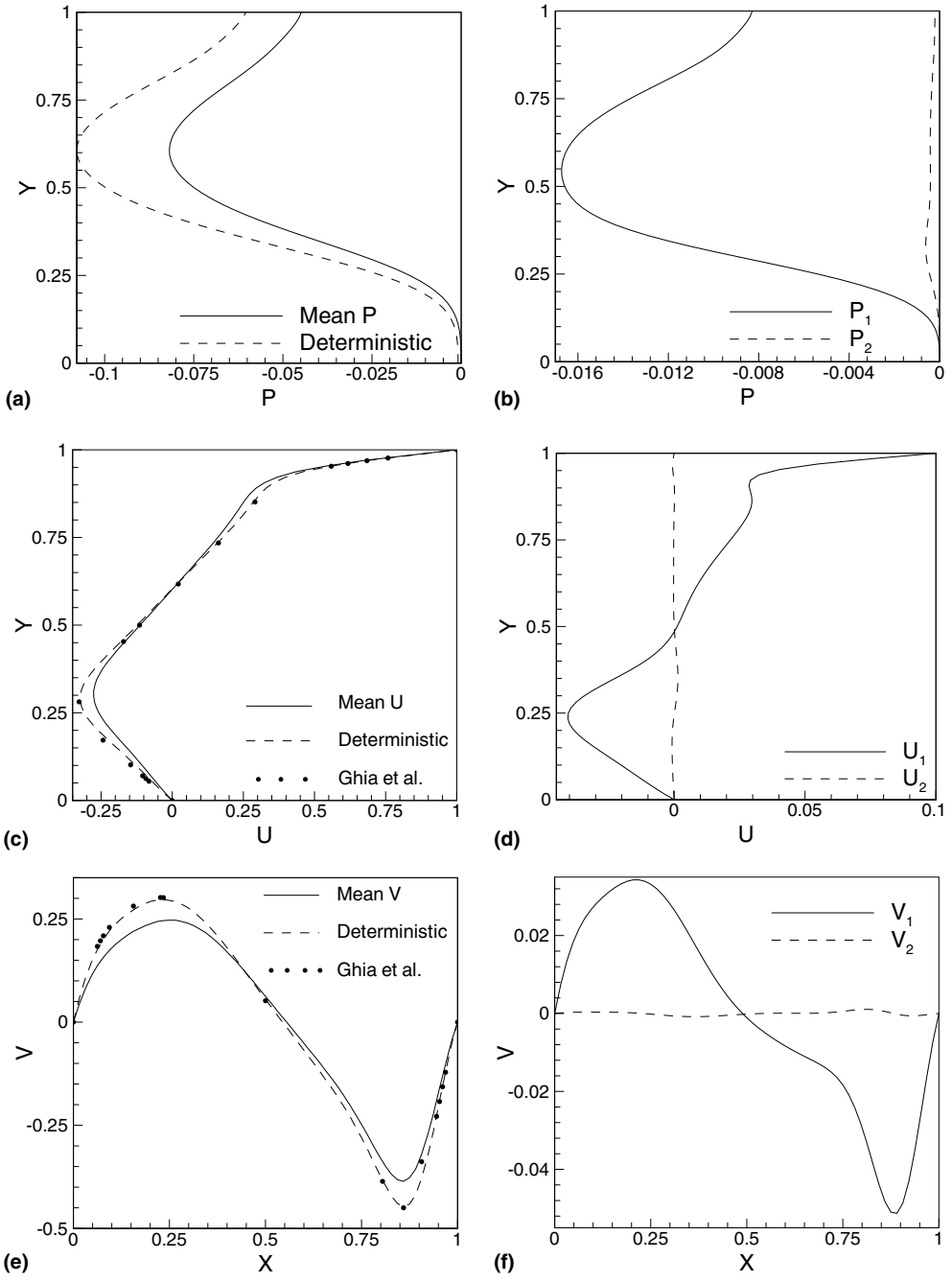

Fig. 13. Lid driven cavity: comparison between mid-plane quantities with deterministic results and plots of higher order coefficients in Legendre chaos expansion of solution at the mid-plane: (a) mid-plane mean pressure; (b) second and third term in LCE expansion of mid-plane pressure; (c) mid-plane mean x-velocity; (d) second and third term in LCE expansion of mid-plane x-velocity; (e) mid-plane y-velocity; (f) second and third term in LCE expansion of mid-plane y-velocity.

recirculation and existence of a center of low pressure makes this problem an ideal choice for uncertainty analysis. The problem definition is depicted in Fig. 12. Uncertainty is considered in the lid velocity. Material parameters like viscosity are taken to be constant and deterministic.

The chief flow characteristics investigated in the problem include: (i) the mean mid-plane pressure versus the deterministic mid-plane pressure; (ii) the mean mid-plane velocity versus the deterministic mid-plane velocity; (iii) the effect of uncertainty on mean flow streamlines at steady-state; (iv) an investigation of recirculation patterns at steady-state.

6.4.1. Computational details

The lid-driven cavity problem is addressed here as a transient problem. The computational domain comprises of 65×65 bilinear quadrilateral elements. The simulation was carried out until steady-state was

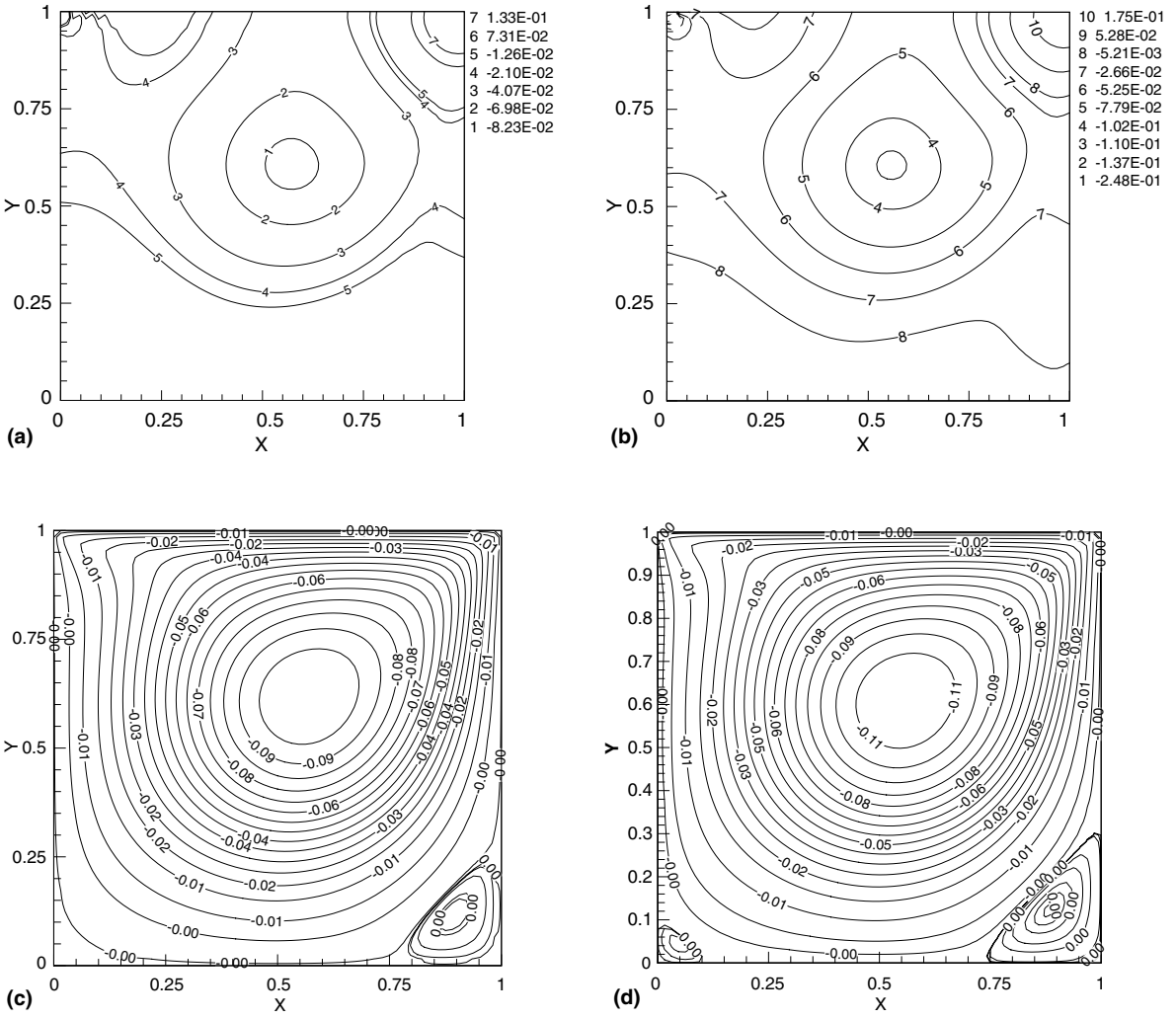

Fig. 14. Lid driven cavity: steady-state contours for (a) the mean pressure, (b) the deterministic pressure, (c) the mean streamlines and (d) the deterministic streamline pattern.

achieved at around $t \approx 20$ s. The lid velocity is modeled as a random variable with a uniform distribution $U[0.9,1.1]$. This amounts to uncertainty level in lid velocity of about 10% of the mean. The kinematic viscosity is deterministic and taken as $v = 0.0025$. Since the uncertainty in lid velocity manifests as uncertainty in Reynolds number, the stochastic simulation tries to capture the effects of a range of flow regimes around a mean Reynolds number of 400 in one simulation.

6.4.2. Discussion of results

Since the lid velocity is modeled as a uniform random variable, Legendre-chaos (LCE) expansions were used to represent the velocity and pressure solutions. For the level of uncertainty considered, the convergence in mean and standard deviation were observed for second-order Legendre-chaos representation. The comparison of mean mid-plane quantities with the deterministic simulation results are shown in Fig. 13. The benchmark solution by Ghia et al. [49] have also been included in Fig. 13(c) and (e). It should be emphasized that the mean flow Reynolds number (here 400) and the Reynolds number used for the deterministic simulations should be the same. It can be observed that the mean stochastic solution is less than the corresponding deterministic solution. This outcome has been attributed to the extra diffusion added due to uncertainty effects [14–16]. Though there is no initial uncertainty in pressure solution, the first-order coefficient in LCE expansion of the pressure is around 16% of the mean pressure. This indicates that the uncertainty propagation in such systems is highly nonlinear and that uncertainty in any input quantity can drastically affect the uncertainty in any other output quantity.

We now compare the mean pressure and mean streamline contours for the stochastic solution and deterministic solution at steady-state. The contours are plotted in Fig. 14. It can be noted that the small recirculation zone at the bottom left of the lid is not captured by the stochastic simulation. Further, the maximum values of the streamfunction are -0.1 for the stochastic solution and -0.112 for the deterministic solution. Ghia et al. [49] provide -0.1139 as the maximum streamfunction value.

6.5. Flow past a circular cylinder – wake flow

This problem is the classical example of flow past bluff bodies. The alternate shedding of vortices in the near wake leads to large pressure fluctuations that can cause structural vibrations and unacceptable noise levels. Hence, the investigation of dynamics in the cylinder wake is an important problem from engineering standpoint.

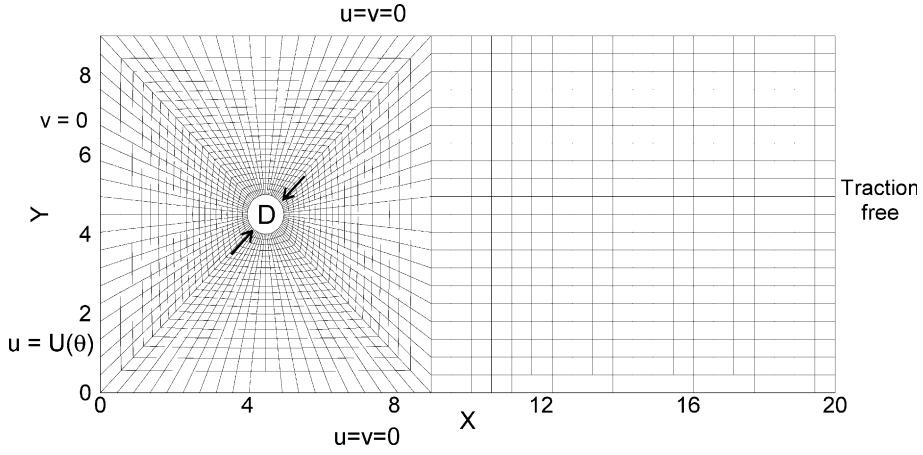

Fig. 15. Problem definition and computational domain for the flow past a circular cylinder example.

nown in Fig. 15. Based on the dimensions sh

D/ν, where U_0 is the far field fluid velocity

ly linked to the Reynolds number. Thus

tern in the cylinder wake. The simulati

In this case, the flow is completely in

shown in Fig. 15 comprises o

$t = 180$ s with a time step

ith a probability distri

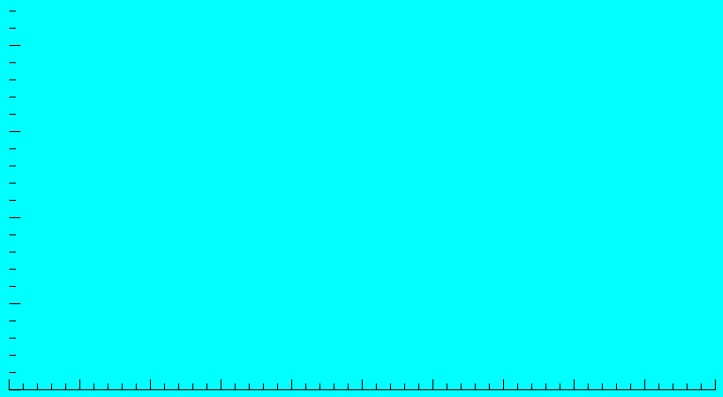

Fig. 16. Flow past

given as $\nu = 0.01$. No uncertainty is considered in the initial conditions. The outflow boundary is assumed to be traction-free.

It is interesting to note that the vortex shedding is initiated by the higher-order terms in the Legendre chaos expansion of the solution (velocity and pressure). Fig. 16(a) and (b) shows that the first-order term in LCE of pressure has already entered the periodic vortex shedding regime when the mean pressure just starts exhibiting the transition to the vortex shedding regime. It is thus very important to ensure that the higher order terms are calculated accurately. Typically, due to the relatively high uncertainty level considered (10% fluctuation about the mean value), the convergence of the solver for higher order terms is severely tested. Typically the number of GMRES restarts were 7–10 times more than the number of restarts in the steady solution regime. The dimension of Krylov subspace for GMRES iterations was doubled from 30 to 60 for the vortex-shedding regime. Further investigation of effective preconditioners for solution of systems arising from the method is warranted.

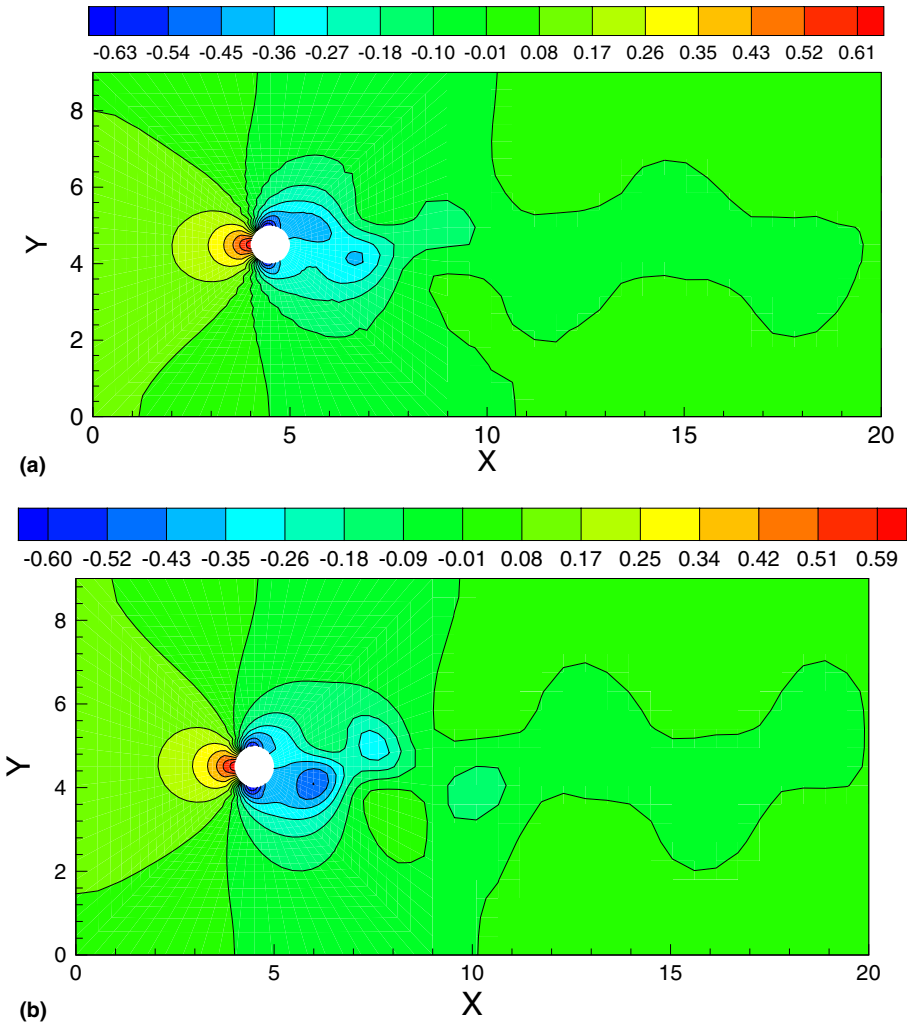

Fig. 17. Flow past a circular cylinder: mean pressure contours at $t = 144$ s (a) stochastic simulation and (b) deterministic simulation.

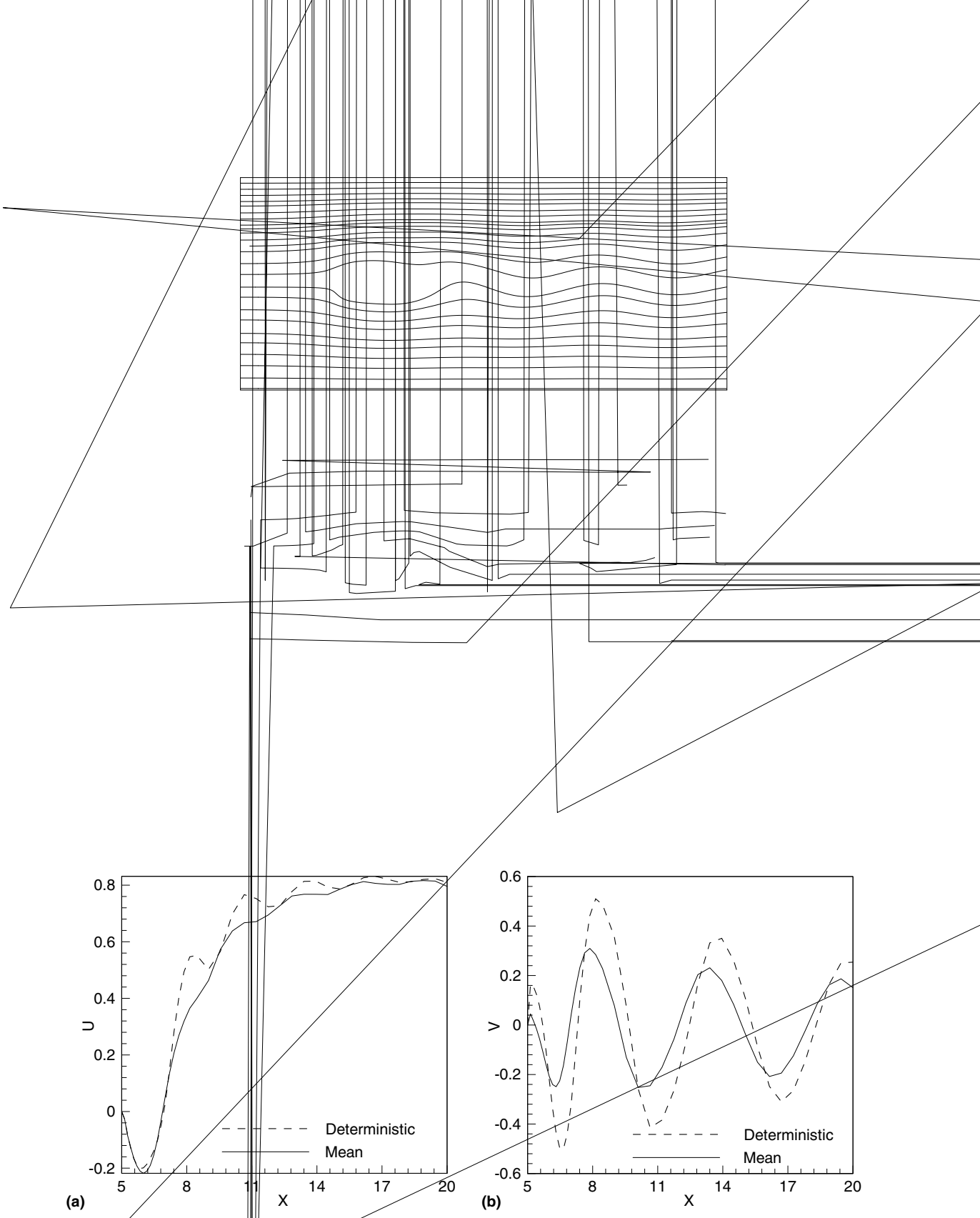

Fig. 19. Flow past a circular cylinder: comparison of deterministic velocity components with the mean of the stochastic velocity components along the centerline in the cylinder wake region.

For the sake of comparing our results with those of a deterministic flow past a circular cylinder simulation we ran a deterministic simulation with Reynolds number 100 and with all other simulation parameters (grid, time stepping) remaining the same. The results at $t = 144$ s are shown in Figs. 17–19. The mean pressure contours at $t = 144$ s in Fig. 17(a) and (b) show interesting details. The stochastic mean pressure is out of phase with the deterministic pressure. This can be noticed by the shedding pattern in the wake region. Further, the near wake effects decay faster for the stochastic mean pressure. This is observed by the decay of eddies nearer to the cylinder than in the case for deterministic simulation. It can be observed that the streamline patterns for mean velocity components Fig. 18(a) and (b) also show considerable difference. Also, the deterministic streamlines indicate a stronger circulation in the near wake region than for the stochastic mean component. This can be argued by the nature of the stochastic velocity behind the cylinder wake. Variation in Reynolds number typically causes a change in the location of vortices behind the cylinder wake. Thus, averaging the velocities obtained over a range of Reynolds numbers will cause the vortices to be smoothed out. The comparison of velocity components for the deterministic simulation and the stochastic simulation are shown in Fig. 19(a) and (b). Again differences can be observed in magnitude and phase in both velocity components. The velocity spectrum calculated using FFT (Fig. 20) of mean velocity is considerably broad. This is in contrast with the deterministic simulations where a sharp shedding frequency is obtained. The dominant frequency however is nearly the same as the deterministic vortex shedding frequency. A value of 0.162 was obtained for the Strouhal number based on mean velocity. This analysis of velocity spectrum is however a guideline and does not explain the essential dynamics of the uncertainty propagation. It can be observed that though the uncertainty in inlet velocity amounts to 10% fluctuation about the mean value, the pressure fluctuation after the onset of vortex shedding is about 35% of the mean value (see Fig. 21(a) and (b)). This stresses the need for maintaining accuracy of the higher-order LCE terms since they are comparable to the mean solution and hence play an essential part in the governing dynamics of the system.

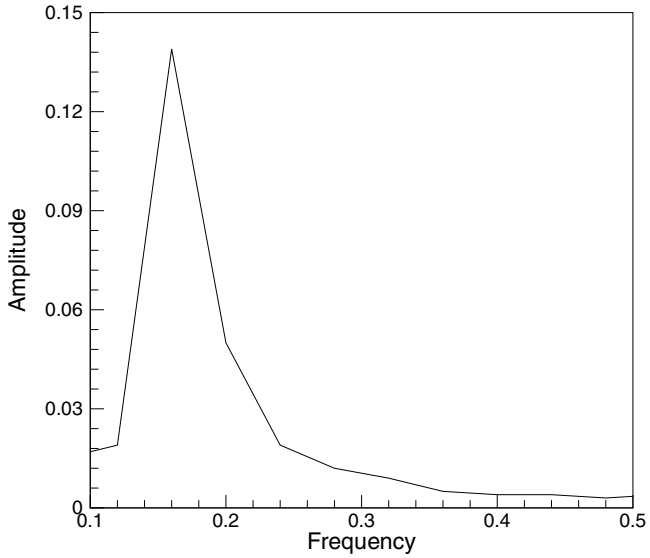

Fig. 20. Flow past a circular cylinder: mean velocity spectrum (dc component not shown).

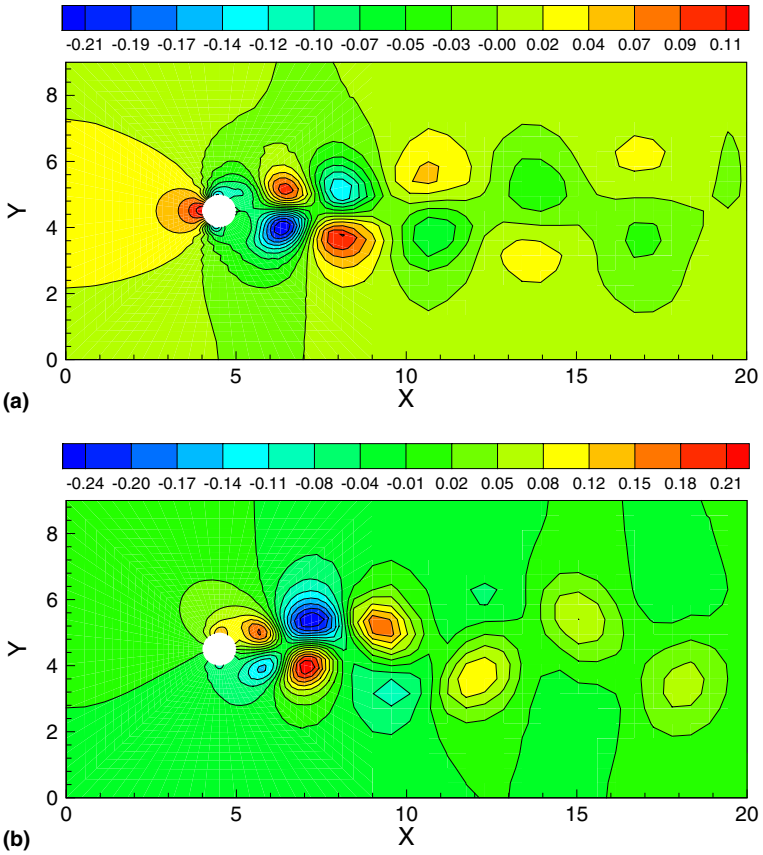

Fig. 21. Flow past a circular cylinder: higher-order Legendre chaos terms for stochastic pressure solution at $t = 144$ s (a) first order term and (b) second order term.

7. Conclusions

A stabilized finite element framework has been developed based on the variational multiscale method with algebraic subgrid modeling for the solution of the linear stochastic scalar advection–diffusion equation and the incompressible stochastic Navier–Stokes equations. Several numerical benchmark examples with uncertainty in boundary conditions were considered to validate the formulation and to test the numerical efficiency of the implementation.

A parallel finite element implementation using cluster specific implementation of BLAS I and BLAS II and a preconditioned parallel GMRES solver with restart capability were developed for parallel solution of the coupled stochastic partial differential equations. Though the computational effort involved with the proposed method is an order of magnitude higher than that of a deterministic problem, it was still found to be two orders of magnitude faster than the Monte-Carlo simulation for advection–diffusion problems.

The computational methodology, however, can be refined in the following areas:

- The convergence rate of the GMRES solver in transient problems like flow past a circular cylinder (on the onset of vortex shedding) went down drastically. New preconditioning strategies need to be developed to this end.

- The solution scheme still suffers from curse of dimensionality. If the input has a steeply decaying covariance kernel, a higher dimensional Askey chaos polynomial representation is needed for the solution. This places a computational constraint on available algorithms.
- Though Askey chaos is well suited for a variety of probability distributions, if the input probability model is derived from experimental data, Askey chaos may not be sufficient to ensure exponential convergence in probability distribution. Some of our current research efforts are addressing these limitations.
- Finally, convergence results for the spectral stochastic finite element method and more specifically for the presented stochastic variational multiscale method have not yet been established. This is an area of significant importance to the future development and use of these techniques.

Acknowledgement

The authors thank the anonymous reviewers for providing detailed and insightful comments that helped us to substantially improve the presentation of this work. The work presented here was funded in part by NASA, Office of Biological and Physical Sciences Research (grant NAG8-1671), the Computational Mathematics program of the Air Force Office of Scientific Research (grants F49620-00-1-0373 and FA9550-04-1-0070) and the Design and Integration Engineering Program of the Design Manufacture and Industrial Innovation Division of the National Science Foundation (grant DMI-0113295). This research was conducted using the resources of the Cornell Theory Center, which receives funding from Cornell University, New York State, federal agencies, and corporate partners.

References

[1] V. Kapoor, L. Gelhar, Transport in three-dimensionally heterogenous aquifers: 1. dymanics of concentration fluctuations, Water Resour. Res. 30 (6) (1994) 1857–1864.
[2] D.T. Burr, E.A. Sudicky, R.L. Naff, Nonreactive and reactive solute transport in three-dimensional heterogenous porous media: mean displacement, plume spreading and uncertainty, Water Resour. Res. 30 (3) (1994) 791–815.
[3] C. Mendoza, T. McAlary, Modeling of ground-water contamination caused by organic solvent vapors, Ground Water 28 (2) (1990) 199–206.
[4] J. Borggaard, D. Pelletier, E. Turgeon, Parametric uncertainty analysis for thermal fluid calculations, Nonlin. Anal. 47 (2001) 4533–4543.
[5] E. Turgeon, D. Pelletier, J. Borggaard, Application of a sensitivity equation method to the k-εmodel of turbulence, in: Proceedings of the 15th AIAA Computational Fluid Dynamics Conference, 2001.
[6] J. Borggaard, J. Burns, E. Cliff, M. Gunzburger, Sensitivity calculations for a 2D, inviscid, supersonic forebody problem, in: H. Banks, R. Fabiano, K. Ito (Eds.), Identification and Control of Systems Governed by Partial Differential Equations, SIAM Publications, Philadelphia, 1993, pp. 14–24.
[7] A. Godfrey, E. Cliff, Sensitivity equations for turbulent flows, in: Proceedings of the 39th AIAA Aerospace Sciences Meeting and Exhibit, AIAA Paper 2001-1060, 2001.
[8] R.G. Ghanem, P.D. Spanos, Stochastic Finite Elements: A Spectral Approach, Springer-Verlag, New York, 1991.
[9] R.H. Cameron, W.T. Martin, The orthogonal development of nonlinear functionals in series of Fourier Hermite functionals, Annal. Math. 48 (1947) 385–392.
[10] O.P. Le Maitre, O.M. Kino, H.N. Najm, R. Ghanem, A stochastic projection method for fluid flow I. Basic formulation, Comput. Phys. 173 (2001) 481–511.
[11] O.P. Le Maitre, M. Reagan, H.N. Najm, R. Ghanem, O.M. Knio, A stochastic projection method for fluid flow. II: Random process, J. Comput. Phys. 181 (2002) 9–44.
[12] O.P. Le Maitre, O.M. Knio, R. Ghanem, H.N. Najm, A stochastic projection method for microchannel flow, Modeling and simulation of microsystems. Available from: www.cr.org, ISBN 0-9708275-0-4, 2001.

[13] R. Ghanem, Probabilistic characterization of transport in heterogenous media, Comput. Meth. Appl. Mech. Eng. 158 (1998) 199–220.
[14] D. Xiu, D. Lucor, C.-H. Su, G.E. Karniadakis, Stochastic modeling of flow-structure interactions using generalized polynomial chaos, J. Fluids Eng. 125 (2001) 51–59.
[15] M. Jardak, C.-H. Su, G.E. Karniadakis, Spectral polynomial chaos solutions of the stochastic advection equation, J. Sci. Comput. 17 (2002) 319–338.
[16] D. Xiu, G.E. Karniadakis, Modeling uncertainty in flow simulations via generalized polynomial chaos, J. Comput. Phys. 187 (2003) 137–167.
[17] T.J.R. Hughes, A.N. Brooks, A multi-dimensional upwind scheme with no crosswind diffusion, in: T.J.R. Hughes (Ed.), Finite Element Methods for Convection Dominated Flows, vol. 34, ASME, New York, 1979 pp. 19–35.
[18] A.N. Brooks, T.J.R. Hughes, Streamline-upwind/Petrov–Galerkin formulations for convective dominated flows with particular emphasis on the incompressible Navier–Stokes equations, Comput. Meth. Appl. Mech. Eng. 32 (1982) 199–259.
[19] T.J.R. Hughes, L.P. Franca, G.M. Hulbert, A new finite element formulation for computational fluid dynamics: VII. The Galerkin least squares method for advective–diffusive equations, Comput. Meth. Appl. Mech. Eng. 59 (1986) 85–99.
[20] T.E. Tezduyar, R. Shih, S. Mittal, S.E. Ray, Incompressible flow using stabilized bilinear and linear equal-order-interpolation velocity–pressure elements, Research Report UMSI 90/165, University of Minnesota Supercomputer Institute, Minneapolis, 1990.
[21] T.J.R. Hughes, Multiscale phenomena: Green's functions, the Dirichlet-to-Neumann formulation, subgrid scale models, bubbles and the origin of stabilized methods, Comput. Meth. Appl. Mech. Eng. 127 (1995) 387–401.
[22] F. Ilinca, J.-F. Hétu, D. Pelletier, On stabilized finite element formulations for incompressible advective–diffusive transport and fluid flow problems, Comput. Meth. Appl. Mech. Eng. 188 (2000) 235–255.
[23] F. Brezzi, L.P. Franca, T.J.R. Hughes, A. Russo, $b = \int g$, Comput. Meth. Appl. Mech. Eng. 145 (1997) 329–339.
[24] J.-L. Guermond, Stabilization of Galerkin approximations of transport equations by subgrid modeling, M2AN 33 (1999) 1293–1316.
[25] G. Haukeand, A. Garcia-Olivares, Variational subgrid scale formulations for the advection–diffusion-reaction equation, Comput. Meth. Appl. Mech. Eng. 190 (2001) 6847–6865.
[26] P. Park, T.Y. Hou, Multiscale numerical methods for singularly-perturbed convection diffusion equations, Intl. J. Comp. Meth. 1 (1) (2004) 1–49.
[27] T.Y. Hou, X.H. Wu, A multiscale finite element method for elliptic problems in composite materials and porous media, J. Comput. Phys. 134 (1997) 169–189.
[28] T.Y. Hou, X.H. Wu, Z.Q. Cai, Convergence of a multiscale finite element method with rapidly oscillating coefficients, Math. Comp. 68 (1999) 913–943.
[29] T.J.R. Hughes, L. Mazzei, K.E. Jansen, Large eddy simulation and the variational multiscale method, Comput. Visual. Sci. 3 (2000) 47–59.
[30] T.J.R. Hughes, A.A. Oberai, L. Mazzei, Large eddy simulation of turbulent channel flows by the variatioanl multiscale method, Phys. Fluid 13 (2001) 1784–1799.
[31] T.J.R. Hughes, L. Mazzei, A.A. Oberai, A. Wray, The multiscale formulation of large eddy simulation: decay of isotropic turbulence, Phys. Fluid 13 (2001) 505–512.
[32] M. Loève, Probability Theory, fourth ed., Springer-Verlag, Berlin, 1977.
[33] S.I. Resnick, A Probability Path, Birkhäuser, Boston, USA, 2001.
[34] N. Wiener, The homogenous chaos, Am. J. Math. 60 (1938) 897–936.
[35] W. Schoutens, Stochastic processes and orthogonal polynomialsLecture Notes in Statistics, vol. 146, Springer-Verlag, New York, 2000.
[36] D. Xiu, G.E. Karniadakis, On the well-posedness of generalized polynomial chaos expansions for the stochastic diffusion equation, SIAM J. Numer. Anal. (submitted).
[37] R. Codina, Stabilized finite element approximation of transient incompressible flows using orthogonal subscales, Comput. Meth. Appl. Mech. Eng. 191 (39–40) (2002) 4295–4321.
[38] R. Codina, Analysis of a stabilized finite element approximation of the transient convection–diffusion equation using orthogonal subscales, Comput. Visual. Sci. 4 (3) (2002) 167–174.
[39] R. James, T.W. Patzek, Multiscale-stabilized finite element method for miscible and immiscible flow in porous media, J. Hydraul. Res. 42 (2004) 131–140.
[40] S.S. Collis, The DG/VMS Method for unified turbulence simulation, AIAA Paper No. 2002-3124, MEMS Preprint No. 2002-029, 2002.
[41] S. Ramakrishnan, S.S. Collis, Variational multiscale modeling for turbulence control, AIAA Paper No. 2002-3280, MEMS Preprint No. 2002-024, 2002.
[42] S.S. Collis, Monitoring unresolved scales in multiscale turbulence modeling, Phys. Fluid 13 (6) (2001) 1800–1806.
[43] A. Russo, Bubble stabilization of finite element methods for the linearized incompressible Navier–Stokes equations, Comput. Meth. Appl. Mech. Eng. 132 (1996) 335–343.

[44] L.P. Franca, T.J.R. Hughes, Convergence analysis of Galerkin least-squares methods for advective–diffusive forms of the Stokes and incompressible Navier–Stokes equations, Comput. Meth. Appl. Mech. Eng. 105 (1993) 285–298.
[45] T.E. Tezduyar, M. Behr, S.K. Aliabadi, S. Mittal, S.E. Ray, A new mixed preconditioning method for finite element computations, Comput. Meth. Appl. Mech. Eng. 99 (1992) 27–42.
[46] T.E. Tezduyar, M. Behr, Finite element solution strategies for large-scale flow simulations, Comput. Meth. Appl. Mech. Eng. 112 (1994) 3–24.
[47] N. Nigro, M. Storti, S. Idelsohn, T.E. Tezduyar, Physics based GMRES preconditioner for compressible and incompressible Navier–Stokes equations, Comput. Meth. Appl. Mech. Eng. 154 (1998) 203–228.
[48] Y. Eguchi, On streamline diffusion arising in Galerkin FEM with predictor/multi-corrector time integration, Int. J. Num. Meth. Eng. 39 (2002) 1037–1052.
[49] U. Ghia, K.N. Ghia, C.T. Shin, High-Re solutions for incompressible flow using the Navier–Stokes equations and a multigrid method, J. Comput. Phys. 48 (1982) 387–411.
[50] O.R. Burggraf, Analytical and numerical studies of the structure of steady separated flows, J. Fluid. Mech. 24 (1966) 113–151.
[51] F. Pan, A. Acrivos, Steady flows in rectangular cavities, J. Fluid. Mech. 28 (1967) 643–655.
[52] J.D. Bozeman, C. Dalton, Numerical study of viscous flow in a cavity, J. Comput. Phys. 12 (1973) 348–363.